Thermodynamics and Kinetics of Adsorption of Platinum dimethyl cyclooctadiene on Resorcinol-formaldehyde Aerogel from Supercritical Carbon Dioxide Solution

by

Nazire Seda Yaşar

A Thesis Submitted to the
Graduate School of Engineering
in Partial Fulfillment of the Requirements for
the Degree of

Master of Science
in
Chemical and Biological Engineering

Koç University
September 2009

Koç University

Graduate School of Sciences and Engineering

This is to certify that I have examined this copy of a master's thesis by

Nazire Seda Yaşar

and have found that it is complete and satisfactory in all respects,
and that any and all revisions required by the final
examining committee have been made.

Committee Members:

_____

Can Erkey, Ph. D. (Advisor)

_____

Yaman Arkun, Ph. D.

_____

Seda Kızılel, Ph. D.

Date: _____

ABSTRACT

The thermodynamics and kinetics of adsorption of platinum dimethyl (cyclooctadiene) ($PtMe_2COD$) on resorcinol-formaldehyde aerogel8 (RFA8) from supercritical carbon dioxide was investigated. An experimental technique was developed for the investigation of adsorption kinetics where the supercritical CO_2 phase was analyzed directly.

In order to investigate the thermodynamics of adsorption, adsorption isotherm of $PtMe_2COD$-$scCO_2$-RFA8 system at 20.7 MPa and 60°C was measured. The adsorption isotherm was represented by Langmuir Model.

For the investigation of the kinetics of adsorption, a mass transfer model was developed. It was seen that the model represented the experimental data fairly well with a fitting error of 7.2 %. Spherical RFA8 particles with changing diameters were synthesized in order to investigate the effect of particle size on the adsorption kinetics. It was seen that the time to reach the adsorption equilibrium decreased by decreasing particle size. The effect the model parameter tortuosity on the adsorption kinetics was also investigated. As the model parameter tortuosity decreased, the time to reach equilibrium decreased.

In this thesis, Pt nanoparticles supported on RFA8 was also prepared. Effect of metal load on the average particle size of the supported nanoparticles was investigated using XRD measurements. Three different metal loaded 10 wt. %, 22 wt. % and 34 wt % particles were prepared and the average particle sizes were found as 2.3 nm, 3.1 nm and 3.9 nm respectively. It was seen that the average particle sizes increased with increasing metal load.

ÖZET

Bu çalışmada, platinyum dimetil siklooctadiyenin ($PtMe_2COD$) resorsinol-formaldehit aerojel8 (RFA) destek üzerine süperkritik karbondioksit ortamında adsorblanmasının termodinamik ve kinetiği incelenmiştir. Süperkritik karbondioksit fazının direk olarak analiz edilebilmesini sağlayan yeni bir deneysel yöntem geliştirilmiştir.

Adsorpsiyon termodinamiğinin incelenmesi için, $scCO_2$-$PtMe_2COD$- RFA8 sisteminin 20.7 MPa ve 60 °C deneysel şartlar altında adsorpsiyon izotermi ölçülmüştür. Langmuir adsorpsiyon izoterm modeli, sistemi tanımlamak için kullanılmıştır.

Adsorpsiyon kinetiğinin incelenmesi için, bir kütle transfer modeli geliştirilmiştir. Geliştirilen kütle transfer modelinin, deneysel veriyi % 7.2 hatayla oldukça iyi şekilde temsil ettiği gözlemlenmiştir. Kinetik deneyleri için resorsinol-formaldehit aerojeller küresel tanecikler olarak sentezlenmiştir. Bu şekilde tanecik boyutunun adsorpsiyon kinetiğine olan etkisi gözlemlenebilmiştir. Adsorpsiyon dengesine ulaşma zamanı tanecik boyutunun artmasıyla artmıştır. Geliştirilen kütle transfer modelinde kullanılan tortuozite parametresinin adsorpsiyon kinetiğine olan etkisi ayrıca incelenmiştir. Tortuozitenin azalmasıyla, adsorpsiyon dengesine ulaşma zamanı azalmıştır.

Bu çalışmada, RFA8 destek üzerine adsorplanmış platinyum metal nanoparçacıkları da ayrıca hazırlanmıştır. Farklı ağırlık yüzdelerinde metal yüklenmiş parçacıkların parçacık boyutları XRD ölçümleri ile elde edilmiştir. Üç ayrı % 10, % 22 ve % 34 metal yüklenmiş nanoparçacıkların parçacık boyutları sırasıyla 2.3 nm, 3.1 nm ve 3.9 nm olarak bulunmuştur. Partikül boyutunun metal yüklemesinin artmasıyla arttığı gözlemlenmiştir.

ACKNOWLEDGEMENTS

First of all, I would like to thank my thesis advisor Professor Can Erkey for his guidance and support during two years of my graduate study. Thanks to him, I was able to participate in international conferences and workshops, write journal papers and also eat fish with colleagues in lovely places of İstanbul. I will always remember him as a kind, generous and friendly advisor.

I would also like to thank Professor Yaman Arkun and Professor Seda Kızılel for their support in my thesis work. Next, I want to thank Professor Mehmet Somer for his tolerance in using his lab and Cevriye Koz for her help in doing XRD measurements.

Then, I thank to my colleagues Seda Giray, Selmi Bozbağ, Erdal Uzunlar and Nil Dinçer for their help in the laboratory. I also want to give my special thanks to Dr. Ayşe Bayrakçeken for her answers and comments for the questions in my research. She was always like a friend for me and never reminding me her dignity. I especially want to thank my colleague Ayşe Meriç Kartal for being not only a partner but also a lovely friend during two years. Most of my hard times would be unbearable without her.

I also want to give my lots of thanks to my old friends Çağrı Dedeoğlu, Esra Satıcı, Serra Caner and Deniz Şanlı. Special thanks to Çağrı for his help in the format of my thesis, Serra and Deniz for being best home mates and Esra for being best friend. I also want to thank my friends Müge Karaman, Musa Özboyacı, Turan Bulmuş, Hakan Doğan, Nihan Çömden and Özge Narin. I have met them here, but I feel like I know them for lots of years. Thanks for making my life more enjoyable.

Finally, I want to thank my parents and my sisters Zeynep and Cansu. I love you very much.

TABLE OF CONTENTS

LIST OF TABLES

LIST OF FIGURES

NOMENCLATURE

T_c	critical temperature
P_c	critical pressure
ρ_c	critical density
q	uptake amount of organometallic precursor on substrate
C	Concentration of organometallic precursor in supercritical phase
K_1	Langmuir adsorption constant
Q_0	Adsorption capacity
N_A	Diffusion flux of the organometallic precursor in supercritical phase to the porous volume in the substrate
k_m	mass transfer coefficient
$D_{e,p}$	effective diffusivity for diffusion in porous catalysts
$F(\lambda)$	size restriction factor
λ	ratio of solute diameter to pore size
ds	solute diameter
dp	pore size of adsorbent particles
ε	porosity of the adsorbent
D_{AB}	binary diffusion coefficient
τ	tortuosity
Sc	Schmidt number at high pressure
$Sc*$	Schmidt number at atmospheric pressure
Sc^+	Schmidt number at high to that at atmospheric pressure
a_i	constant in correlation of Schmidt number with solvent molar volume
υ_0	hard sphere closest packed volume of solvent molecules
υ	molar volume of solvent
c_i	constant in correlation of Schmidt number with effective hard sphere packed volume

σ_1	hard sphere diameter of the solute
σ_2	hard sphere diameter of the solvent
M_1	molecular weight of the solute ($PtMe_2COD$)
M_2	molecular weight of the solvent ($scCO_2$)
$C_{A,s}$	concentration of $PtMe_2COD$ in the supercritical phase at the surface of the adsorbent
$C_{A,b}$	concentration of $PtMe_2COD$ in the bulk supercritical phase
t	time
V	volume of $scCO_2$
C_{A0}	initial concentration of $PtMe_2COD$ in $scCO_2$ at t=0
ρ_p	density of porous substrate particles
S	external surface area of the substrate particles
d_{XRD}	XRD average particle size of the metallic nanoparticles
λ_w	wavelength of X-ray
$\beta_{1/2}$	width of the peak at half height
θ	angle at the peak maximum

Chapter 1

INTRODUCTION

A nanoscale composite material is defined as a material that has a structure such that at least one of its phases has one or more dimensions (length, width, or thickness) in the nanometer size range, usually ranging from 1 to 100 nm. Such materials include polycrystalline materials with nanometer sized crystallites, materials with surface protrusions spatially separated by distances on the order of nanometers, granular or porous materials with grain sizes in the nanometer range or nanometer sized metallic clusters dispersed within a porous matrix (supported metal nanoparticles). Among these materials, supported metal nanoparticles have attracted a great deal of interest for microelectronic, optical and catalytic applications because of their unique properties which are directly related to the specific particle morphology (size and shape), metal dispersion, concentration and the electronic properties of the metal within their host environment [1].

In the preparation of supported metal nanoparticles, various types of inorganic or organic substrates can be used. Carbon supports are widely used as inorganic substrates whereas polymeric supports are used as the organic substrates. Many studies were done for the preparation of carbon supported nanoparticles which are mostly used as catalysis in hydrogenation reactions [2,3], oxygen reduction reactions (ORR) in electrochemical fuel cells [4] or catalytic oxidation of sulfur dioxide in exhaust gas treatment [3]. Moreover, many studies were also done by using organic polymeric substrates in preparation of supported nanoparticles which are mostly used as catalysis for various type of reactions [5, 6, 7, 8].

There are various ways of synthesizing metal nanoparticles, with diameters between 1-20 nm. These include deposition-precipitation, impregnation, sol-gel [9], sonochemical [10], chemical vapor impregnation [11], microemulsion using stabilizing agents [12]. However for all of these methods there are some limitations. In these methods, it is difficult to control the particle size, distribution and the metal concentration in the materials [13]. Moreover, these methods are not easily applicable to polymeric substrates [13].

Supercritical fluid deposition (SCFD) is a relatively new method for preparation of supported nanoparticles. SCFD consists of a series of steps which are the dissolutioning of a metallic precursor in a SCF, the exposure of a porous substrate to the solution, adsorption of the precursor on the surface of the support and finally the reduction of the precursor to its metal form. This technique has been used to prepare various metallic nanoparticles supported on different types of polymers. The first study on preparation of polymer supported nanoparticles was published by Watkins and McCarthy [14]. Platinum dimethyl cyclooctadiene was impregnated into poly(4-methylpent-1-ene) (PMP) and poly (tetrafluoroethylene) (PTFE) from a $scCO_2$ solution at 80 $^{\circ}$C and 15.5 MPa for 4 h. Subsequent reduction of the precursor resulted in discrete platinum clusters in PMP having maximum diameters of approximately 15 and 50 nm depending on the reduction method. This study was followed by numerous studies where polymer supported nanoparticles was synthesized by SCFD [15,16,17, 18,19].

In the preparation of supported nanoparticles by using SCFD, the adsorption process which the metallic precursor adsorbs on the surface of the support plays an important role. The adsorption process in SCFD consists of a series of steps such as external mass transfer of the precursor from the supercritical fluid phase to the surface of the adsorbent, diffusion of the precursor in the pores of the adsorbent, adsorption of the precursor onto the surface of the adsorbent and surface diffusion within the adsorbent. The rates of dissolutioning and reduction of the precursor are fairly fast processes and

therefore the rate of deposition is primarily controlled by the rate of adsorption of metallic precursors [20].

Unfortunately, our understanding of adsorption of organometallics on the surfaces of porous supports from SCF solutions is very limited. In one of the few studies carried out in this area, Zhang et al. investigated the thermodynamics and kinetics of the adsorption of bis (2,2,6,6-tetramethyl-3,5-heptanedionato) (1,5-cyclooctadiene) ruthenium (II) ($Ru(cod)(tmhd)_2$) on carbon aerogel from supercritical CO_2 ($scCO_2$) solutions [21]. Using batch adsorption experiments, they determined the adsorption isotherms of ($Ru(cod)(tmhd)_2$) at various temperatures and pressures and found that the isotherms were represented by the Langmuir model. The kinetics of adsorption could be predicted using a model consisting of coupled partial differential equations based on diffusion in the pore volume and assuming local equilibrium at the adsorbent – fluid interface within the pores. Saquing et al. [22] measured the adsorption isotherm of platinum dimethyl cyclooctadiene ($PtMe_2COD$) on carbon aerogels in the presence of $scCO_2$ and the Langmuir model was found to fit the data satisfactorily. Recently, Aschenbrenner et al. [23] studied the thermodynamics and kinetics of adsorption of $PtMe_2COD$ on two porous supports, silica gel tablets and a monolithic cordierite. They developed a new experimental technique which involved circulating a solution of known concentration of $PtMe_2COD$ in $scCO_2$ over the porous support in a closed system. The fluid phase concentration was determined by UV spectroscopy as a function of time and the uptake was determined from the difference of initial amount of $PtMe_2COD$ placed in the system and the amount of $PtMe_2COD$ in the fluid phase. Equilibrium was reached very fast in (1 to 2) h with monolithic cordierite whereas times longer than several hours were required for silica gel tablets. Accurate determination of uptake at longer times was not possible due to a drift in the baseline signal of the detector.

In the experiments carried out by Zhang et al. [21] and Saquing et al.[22] , the uptake values were determined after depressurization of the fluid phase. During depressurization, some of the adsorbed organometallic compound may be expelled from

the support, may desorb because of a shift in equilibrium or some of the organometallic compound in the fluid phase may precipitate on the support. Consequently, the measured uptake values may not be accurate. Along similar lines, the experiments conducted by Aschenbrenner et al. [23] showed differences of up to 50 % between uptake values determined by weighing the sample after depressurization and determined from the fluid phase concentration before depressurization.

In this study, Pt nanoparticles supported on resorcinol-formaldehyde aerogels (RFA) which is a polymer was synthesized through supercritical carbon dioxide deposition using a newly developed experimental technique. Platinum dimethyl cyclooctadiene ($PtMe_2COD$) was used as the organometallic precursor. The RFA support was synthesized with an average pore size of 8 nm (RFA8) and its pore properties and surface area was determined by using BET analysis. The total BET surface area of RFA8 was found as 759 m^2/g. The total pore volume of RFA8 was found as 2.5 m^3/kg. The preparation of Pt/RFA8 nanoparticles involved the adsorption of $PtMe_2COD$ on RFA8 from $scCO_2$ solution and the subsequent thermal reduction of $PtMe_2COD$ to Pt. The effect of metal load on the size and distribution of the Pt particles on RFA8 was investigated by using XRD and TEM measurements.

The study was primarily on the investigation of the thermodynamics and kinetics of adsorption of $PtMe_2COD$ on the surface of RFA8. The thermodynamics of adsorption is described by the equilibrium adsorption isotherm of the $PtMe_2COD$-$scCO_2$-RFA8 system at the adsorption conditions. This adsorption isotherm gives the relation between the concentration of $PtMe_2COD$ in $scCO_2$ and the uptake amount of $PtMe_2COD$ on RFA8 at the equilibrium conditions. The adsorption isotherm was measured at 20.7 MPa and 60°C. The kinetics of adsorption of $PtMe_2COD$ on RFA8 at 20.7 MPa and 60°C was investigated by using an adsorption kinetics model which was recently developed by Zhang et al. in order to describe the kinetics of adsorption of $Ru(cod)(tmhd)_2$ on carbon aerogel [21].

Chapter 2 gives a literature review about the adsorption phenomenon, adsorption isotherms and methods to measure adsorption isotherms. It also includes information about the SCFD method.

Chapter 3 describes the experimental methods of the study, which includes the experiments of the synthesis of the RFA8, the adsorption isotherm measurements, the adsorption kinetics measurements and the preparation of the Pt/RFA8 particles.

The results and discussion of the conducted experiments were given in Chapter 4. The adsorption isotherm of $PtMe_2COD$-$scCO_2$- RFA8 system, the adsorption kinetics data for $PtMe_2COD$-$scCO_2$- RFA8 system and also the XRD results of the prepared Pt/RFA8 particles were represented.

The summary of the work and the future research work was included at the end of the thesis.

Chapter 2

LITERATURE REVIEW

2.1. Supercritical Fluid Deposition (SFD)

2.1.1. Supercritical Fluids

A substance is called a supercritical fluid when it is simultaneously heated and compressed above its critical temperature and critical pressure (T_c, P_c) and is maintained there. General P-T diagram of a pure substance which is given in Figure 2.1 can be used to demonstrate the supercritical region. The three solid lines shown in the figure represents the distinct phase boundaries of the three common states of matter-solid, liquid and gas. Along these lines, two phases are in equilibrium and the three phases coexist at the triple point. The discontinuous transition from liquid to gas terminates at the critical point (T_c, P_c). In the supercritical region, no phase boundaries exists, meaning that in the supercritical region, only a single homogenous phase exists regardless of pressure and temperature. Therefore, it is possible for a substance to cross from a liquid state to the gas state without any phase transition (in this case boiling) by passing through the supercritical region.

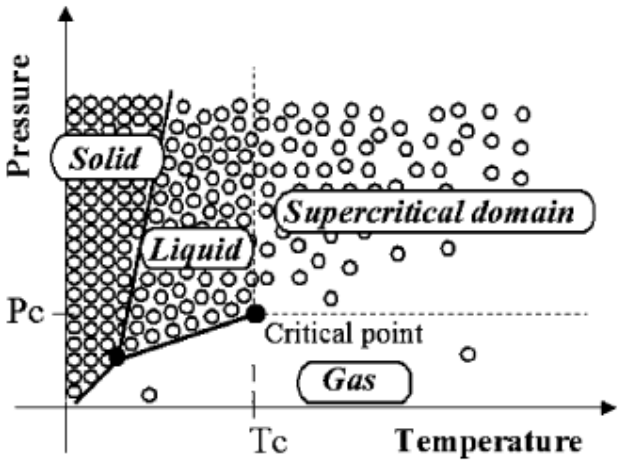

Figure 2.1: The pressure-temperature diagram of a pure substance [24]

The properties of a supercritical fluid are governed primarily by its density which is a strong function of both temperature and pressure. The density which defines the solvent power of a substance is very flexible in supercritical fluids with respect to pressure and temperature. Close to the critical point, a very little change in either pressure or temperature can result in large changes in density; hence this solvating power as well as selectivity which are the crucial parameters for extraction and deposition processes can be altered over a wide range. This feature is what makes a supercritical fluid unique from conventional liquid solvents. In the supercritical region, the thermophysical properties of a substance include liquid-like densities, gas-like viscosities and kinematic viscosities and much higher diffusivities than liquids [24]. A comparison of the properties of common supercritical fluids with that of liquids and gases are given in Table 2.1.

Table 2.1: Comparison of the physical properties of gases, liquids and SCFs [25]

Fluid	**Liquid**	**Supercritical Fluid**	**Gas**
Density (ρ) (kg/m^3)	1000	100-800	1
Viscosity (η) (Pa.s)	10^{-3}	10^{-4}-10^{-5}	10^{-5}
Diffusion coefficient	10^{-9}	10^{-8}	10^{-5}

Supercritical fluids can be used to conduct many processes which can be applied in many fields such as analytical and preparative separations, organic and inorganic synthesis, waste management, material processing (nanomaterials, nanostructured materials, thin films, coating), porous materials and earth science (volcanism, geothermal energy, hydrothermal synthesis) [24].

Table 2.2 gives the critical properties (T_c,P_c,ρ_c) of some pure components which can be utilized in their supercritical state. As it is seen from the table, among the supercritical fluids, supercritical carbon dioxide ($scCO_2$), with a readily accessible T_c of 31 $^{\circ}$C and a P_c of 7.38 MPa, is particularly attractive since it is abundant, inexpensive, non-flammable, non-toxic, and environmentally benign and leaves no residue in the treated medium. Besides the environmental benefits, $scCO_2$ displays high permeation rate in virtually all polymers and the exposure to $scCO_2$ results in various extents of swelling and enhanced chain mobility of the polymers, which makes it possible to incorporate metallic precursors into various polymers. Moreover, the degree of polymer swelling, diffusion rates within the substrate, and the partitioning of precursors between the SCF and the swollen polymer can be controlled by density mediated adjustments of solvent strength via changes in temperature and pressure [13].

Table 2.2: Critical coordinates of usual pure fluids [25]

Fluid	**T_c (°C)**	**P_c (MPa)**	**ρ_c (kg/m^3)**
Carbon dioxide	31.2	7.38	468
Ammonia	132.4	11.29	235
Water	374.1	22.1	317
Ethylene	9.5	5.06	220
Ethane	32.5	4.91	212
Propane	96.8	4.26	225
n-Pentane	196.6	3.37	232
Cyclohexane	279.9	4.03	270
Methanol	240	7.95	275
Ethanol	243.1	6.39	280
Isopropanol	235.6	5.37	274
Acetone	235	4.76	273

2.1.2. Preparation of Supported Metal Nanoparticles by scCO$_2$ deposition

There are several techniques to prepare supported metallic nanoparticles such as impregnation, deposition-precipitation, sol-gel and chemical vapor deposition. However, in all of these techniques there are some drawbacks such as controlling the particle size and distribution, and also the metal concentration in the materials. For example in sol-gel method, the metallic precursor in the solution may interfere with the polymerization chemistry where the materials with undesirable pore properties can be obtained. Moreover, for the conventional co-precipitation, deposition-precipitation and impregnation methods, using liquid solutions which have very high surface tensions as

the processing medium can cause not only the agglomeration of the particles but also the collapse of the fragile supports such as silica aerogels or other organic aerogels.
In chemical vapor deposition method, the limitations are the vapor pressure of the metallic precursor, the processing temperature requirements and the mass transfer-limited kinetics [13].

Supercritical fluid deposition (SFD) method, alternative to the above methods is attractive and promising for the deposition of metallic nanoparticles on the surfaces of porous supports or within polymers. Among the supercritical fluids, supercritical CO_2 is the most commonly used fluid in this method due to its many advantages which are explained in detail in section 2.1.1.

SFD method can be described by three successive steps,

1. The dissolution of a organometallic precursor in the supercritical fluid
2. Adsorption of the metallic precursor on the surface of a porous support from supercritical fluid
3. The reduction of the adsorbed organometallic precursor to its metal form

The above three steps can be represented by a schematic diagram which is seen in Figure 2.2. In the first step, the organometallic precursor that is to be adsorbed is dissolved completely in the supercritical fluid. Subsequently, the dissolved organometallic adsorbs on the surface of the pores of the adsorbent (step 2). After the completion of the adsorption process, the adsorbed organometallic compound is reduced to its metal form by various reduction methods. Reduction process can be conducted either before depressurization of the supercritical fluid or after depressurization of the supercritical fluid. Before depressurization, the organometallic compound can be reduced chemically with H_2 at the supercritical media or reduction can be conducted by thermal treatment in the supercritical media. If the reduction is to be conducted after depressurization of the supercritical fluid, then under atmospheric conditions, chemical reduction with H_2 under heat treatment or thermal reduction at an inert atmosphere can be conducted. However, the dissolutioning and the reduction steps of the SFD method are relatively fast processes and therefore the rate of deposition is

primarily controlled by the rate of adsorption. Thus, the adsorption of the metallic precursor on the surface of the pores of the substrate from a supercritical solution is the controlling phenomenon in the preparation of nanoparticles by SFD method and should therefore be investigated.

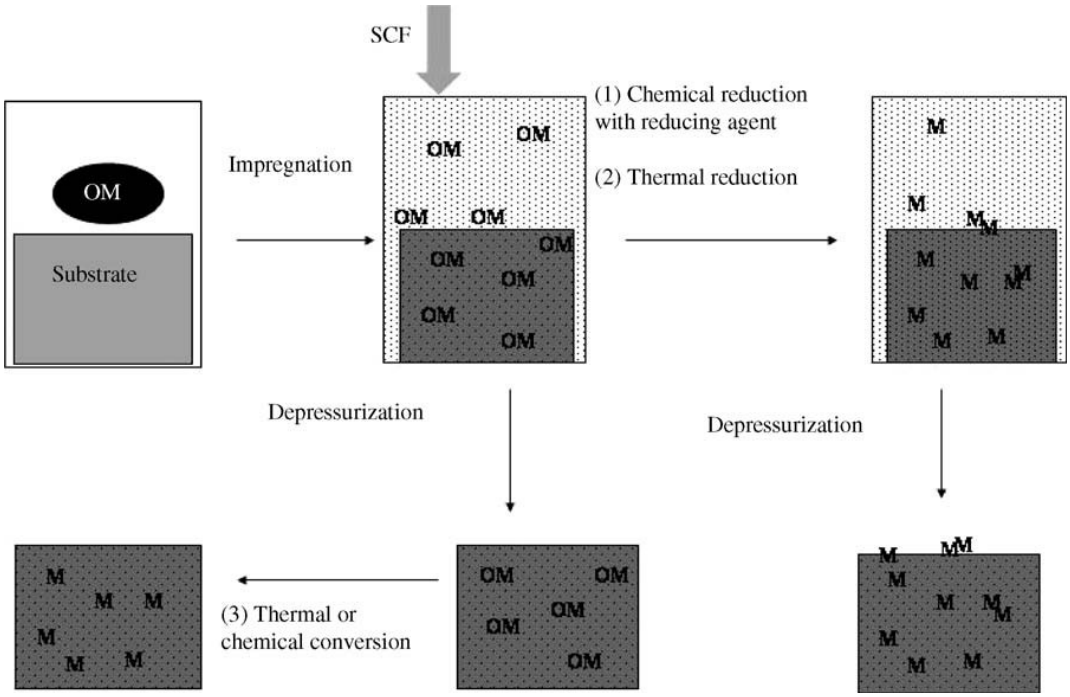

Figure 2.2: Schematic representation of supercritical fluid deposition method [20]

The adsorption of an organometallic precursor on the surface of a porous support is described through four different steps which are the external mass transfer of the organometallic precursor to the external surface of the support, the internal diffusion of the organometallic precursor in the pores of the support, the adsorption of the organometallic precursor on the surface of the pores of the support and the surface diffusion of the adsorbed organometallic. These steps are represented schematically in

Figure 2.3. A spherical porous adsorbent is given in the figure. It can be said that the pores of the adsorbent compare to the cavities that form when the beads of a necklace are held together. The porous adsorbent is in the supercritical medium and the two phases, the supercritical fluid and the solid (adsorbent) phases exist. The concentrations of the organometallic in the bulk supercritical fluid, in the surface of the adsorbent and in the pores of the adsorbent in the radial direction are represented as $C_{A,bulk}$, $C_{A,\ surface}$ and $C_{A,\ r}$ respectively.

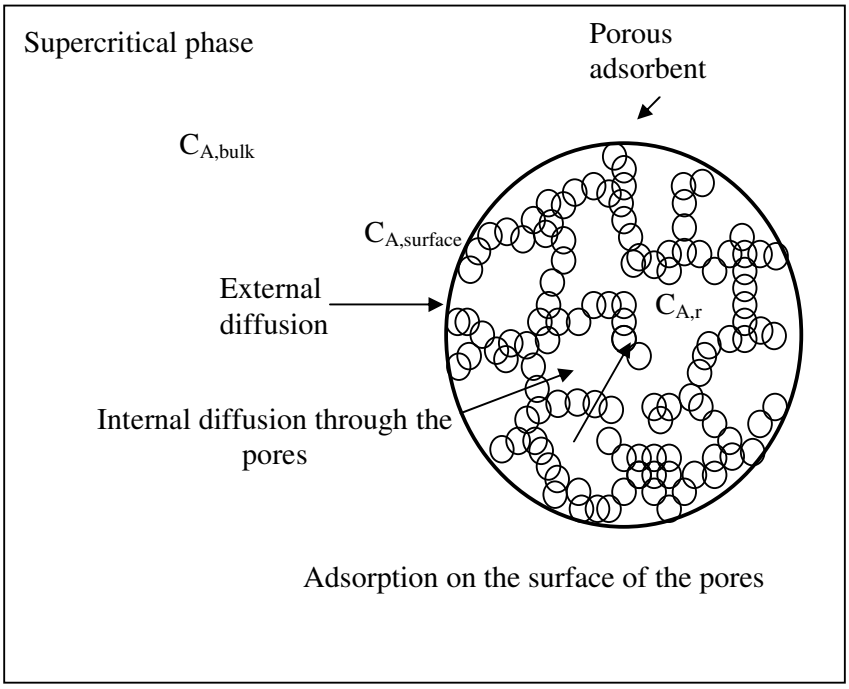

Figure 2.3: Schematic representation of the adsorption from supercritical phases

The adsorption process occurs for the organometallic precursor to reach equilibrium between the fluid (supercritical) phase and the solid (adsorbent) phase. Considering the whole adsorption process, there are two important phenomenons, the thermodynamics of adsorption and the kinetics of adsorption. The thermodynamics of adsorption is described through adsorption isotherms. These isotherms give the relation between the

fluid phase concentration and the solid phase concentration at equilibrium. It is necessary to measure adsorption isotherms in order to understand the adsorption capacity of the adsorbent and also the effect of adsorption conditions on the adsorption capacity of the adsorbent. The kinetics of adsorption can be described by developing kinetic models. Thus, both the thermodynamics and kinetics of adsorption should be investigated in order to understand the whole adsorption process.

In this thesis, the thermodynamics of adsorption of $PtMe_2COD$ (organometallic) on RFA8 (porous adsorbent) from $scCO_2$ was investigated by measuring the adsorption isotherm of the system. The kinetics of adsorption was also determined and investigated with the help of a kinetic model. In the following sections, literature background information will be given about the adsorption phenomenon. Then, considering the thermodynamics of adsorption from supercritical phases, the adsorption isotherm models and previous experimental studies to measure the adsorption isotherms will be given. The very few studies about the investigation of the kinetics of adsorption will also be discussed.

2.2. Thermodynamics of Adsorption

2.2.1. Fundamentals for adsorption from supercritical phases

Adsorption is the selective transfer of certain components of a fluid phase, called solutes to the surface of an insoluble solid. The solid material is referred to as adsorbent, while the adsorbed compounds (adsorpt) together with the adsorbent as adsorbates (Figure 2.4). When adsorbent is exposed to a fluid phase molecules in a gas or liquid or supercritical phase diffuse to its surface (including its pores if it is a porous adsorbent), where they chemically bond with the solid surface or are held there physically by van der Waals forces. Interaction between the surface molecules of the adsorbent and molecules of the fluid phase determine the adsorption equilibrium. If the interaction forces between the surface and fluid molecules are of physical forces i.e. van

der Waals forces, then adsorption is referred to as physical adsorption or physiisorption, whereas if the interaction forces are of chemical forces, then it is called chemical adsorption or chemisorption.

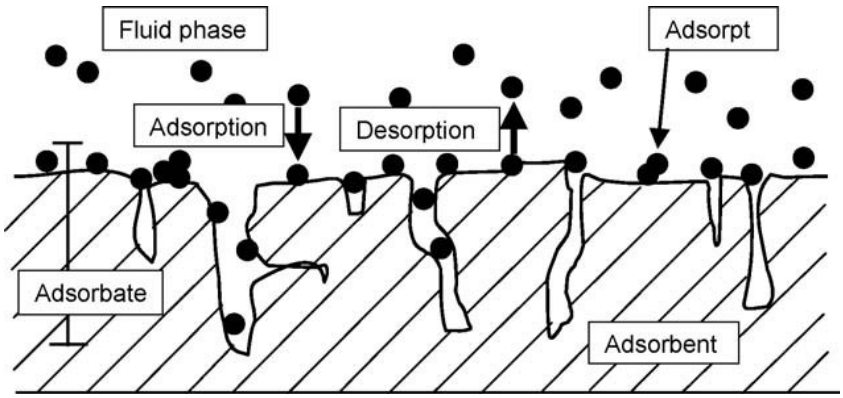

Figure 2.4: Representative picture for adsorption on the surface of a solid [26]

2.2.2. Adsorption Isotherms

In order to describe the adsorption of a component from a fluid phase to the adsorbent, simple and semi-empirical equations are applied since a thermodynamic description of the surface of the adsorbent is not available for practical purposes. The so-called adsorption isotherms relate the loading of the adsorbent to the concentration of the adsorbing compound in the fluid phase at equilibrium.

The simplest form of an adsorption isotherm is a linear equation which can be given as,

$$q_i = KC_i \tag{2.1}$$

where q_i is the amount of the adsorbate i on the adsorbent and C_i is the concentration of i in the fluid phase. K is the constant adsorption coefficient. However, linear adsorption isotherms are applied only in cases where the concentrations are very low.

The nonlinear behavior of adsorption equilibrium isotherms are described by a number of well known equations such as Langmuir-equation, Freundlich equation and the BET equation. Figure 2.5 gives the four types of adsorption isotherms which are basically linear and nonlinear isotherms. Those which are nonlinear can be described through three different curves, convex, concave or quadratic.

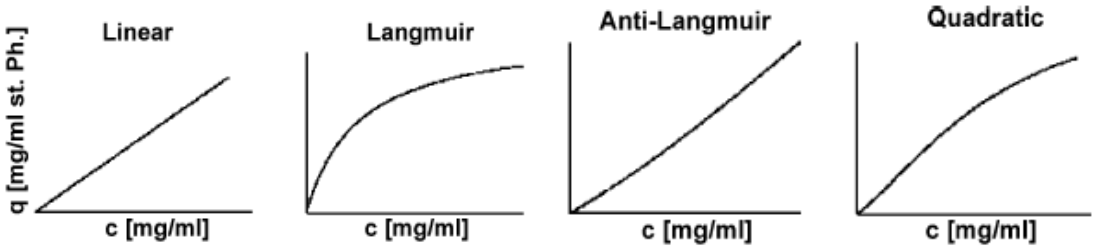

Figure 2.5: Four common types of adsorption isotherms [26]

2.2.3. Adsorption Isotherm Models

2.2.3.1. The Langmuir Model

Langmuir was the first person to propose a coherent theory of adsorption onto a flat surface based on a kinetic viewpoint. He suggested that there is a continual process of bombardment of molecules onto the surface and a corresponding evaporation (desorption) of molecules from the surface to maintain a zero rate of accumulation at the surface at equilibrium. The assumptions of the Langmuir model are:

1. Surface is homogenous, that is adsorption energy is constant over all sites.
2. Adsorption on surface is localized, that is adsorbed atoms or molecules are adsorbed at definite, localized sites.
3. Each site can accommodate only one molecule or atom.

The Langmuir theory is based on a kinetic principle, that is the rate of adsorption is equal to the rate of desorption from the surface. Using the kinetic theory of gases (KTG), the rate of adsorption is directly proportional to pressure (or concentration) and the fraction of the bare sites (θ_0), thus

$$N_{ads} = kP\theta_0 A_1 \tag{2.2}$$

where A_1 is the condensation coefficient and represents the probability of a molecule being adsorbed upon collision with the surface, P is the adsorbate pressure. k is a constant equal to $N_{avo}/ (2\pi MRT)^{1/2}$ where N_{avo} is the Avagadro's number, M is the adsorbate molecular weight, R is the gas constant and T is the absolute temperature. On the other hand, the rate of desorption is proportional to the number of molecules adsorbed and the energy of adsorption, E

$$N_{des} = n_m \theta_1 \nu_1 e^{-E/RT} \tag{2.3}$$

where n_m is the number of adsorbate molecules in a completed monolayer, θ_1 is the fraction of occupied sites and ν_1 is the vibrational frequency of the adsorbate normal to the surface when adsorbed. The term $e^{-E/RT}$ represents the probability that an adsorbed molecule possesses adequate energy to overcome the net attractive potential of the surface. At equilibrium, the rates of adsorption and desorption are equal, thus equating Equations 2.2 and 2.3 and recognizing that $\theta_0=1- \theta_1$, yields

$$kPA_1 - \theta_1 kPA_1 = n_m \theta_1 \nu_1 e^{-E/RT} \tag{2.4}$$

Then solving for θ_1,

$$\theta_1 = \frac{kPA_1}{n_m \nu_1 e^{-E/RT} + kPA_1} \tag{2.5}$$

Allowing

$$K = \frac{kA_1}{n_m \nu_1 e^{-E/RT}} \tag{2.6}$$

Then,

$$\theta_1 = \frac{KP}{1+KP} \tag{2.7}$$

The adsorption energy E is taken constant in equation 2.5 which assumes surface homogeneity (all adsorption sites are energetically identical) and the absence of lateral interactions between adsorbed molecules. A large value of K indicates strong adsorption bonding and the larger the value of K, the greater is the fractional surface coverage at fixed T and P values, or the higher is the temperature required for a specified fractional surface coverage at a fixed P. At low values of P, the fraction of the sites covered is directly proportional to P, but at high values of P, the fraction approaches unity asymptotically and becomes essentially independent of P [27].

2.2.3.2. The Freundlich Model

The Freundlich equation is originally an empirical expression that describes an adsorption isotherm where there is a linear correlation for adsorption capacity as a function of adsorbate pressure (or concentration) when this relationship is plotted on log log scales. The equation is given by:

$$n = KP^a \tag{2.8}$$

where n is the amount of the solute adsorbed per unit amount of adsorbent used, K and a are empirical constants and P is the equilibrium partial pressure (or concentration) of the adsorbate in the bulk phase. The empirical constants in equation 2.7 are determined by fitting the adsorption data to the linear form of the Freundlich equation where the line has a slope of a and intercept of log (K). The Freundlich equation is one of the most common adsorption isotherms.

2.2.3.3. The Langmuir- Freundlich (Sips) Model

This model is similar to Langmuir model but it includes an additional parameter n as in the Freundlich model and is given by:

$$\theta = \frac{(KP)^a}{1+(KP)^a} \tag{2.9}$$

When a = 1, the Sips equation reduces to the Langmuir equation which is expressed for ideal surfaces. The parameter a is included in order to take into account the heterogeneity of the system which is caused by the adsorbent, adsorbate or by a combination of them. The Sips adsorption isotherm gives a similar curve to Freundlich adsorption isotherm, however, in Sips isotherm; there is a saturation limit when the concentration increases. Sips isotherm has a disadvantage similar to Freundlich isotherm, which is a lack of accuracy in dilute regime [28].

2.2.3.4. The Toth Model

One empirical equation that usually gives correct limits at both low and high concentrations is the Toth equation that was developed to represent the adsorption of a monolayer, but with an energetic heterogeneity of the adsorption sites.

$$\theta = \frac{kP}{(1+(kP)^t)^{1/t}} \tag{2.10}$$

where t is the parameter that characterizes the heterogeneity of the system similar to the Sips model [28].

2.2.3.5 The Hill Model

The Hill-isotherm was derived from statistical thermodynamics and is given by the equation below.

$$q = \frac{q_s}{N}\frac{b_a C + 2b_b C^2 + ... + nb_N C^N}{1 + b_a C + b_b C^2 + ... + b_n C^N} \tag{2.11}$$

The parameters of b must be fitted to experimental data. For *N*= 1, this model becomes equal to the Langmuir-isotherm. The loading of the adsorbent approaches to saturation loading q_s at high concentrations [26].

2.2.4. Experimental Methods to Measure Adsorption Isotherms from Supercritical Solutions

The measurement of the adsorption isotherms can only be achieved by conducting experiments. There are several experimental studies conducted so far in order to determine the adsorption isotherms of several systems. Since our study is based on the adsorption of an organometallic compound onto a porous substrate from a $scCO_2$, the studies which give the experimental methods in order to measure adsorption isotherms for $scCO_2$- adsorbate-adsorbent systems will be given.

The methods to measure adsorption isotherms can be classified as dynamic and static methods.

2.2.4.1. Dynamic Methods

Several studies have been published so far for the measurement of the adsorption isotherms in supercritical fluid-solid systems using dynamic methods. Dynamic methods are basically carried out in experimental set ups derived from chromatographic equipment. Dynamic methods can be classified by three different methods which are the determination of the adsorption isotherms by breakthrough curves, perturbation method and the elution by characteristic point (ECP) method. The studies about the determination of the adsorption isotherms using the above methods are discussed below.

2.2.4.1.1. Determination of the Adsorption Isotherms from Breakthrough Curves

Akgerman's group reported the first studies on determination of the adsorption isotherms for supercritical fluid-solid systems from breakthrough curves using frontal analysis chromatography [29, 30, 31]. In a typical frontal analysis method, the supercritical fluid phase containing a certain concentration of the adsorbate is passed over an adsorption column where the adsorbent is packed inside the column. The concentration of the adsorbate in the fluid at the outlet of the column is monitored using a UV detector. The fluid phase is passed through the column until outlet concentration becomes equal to the inlet concentration meaning that the adsorption equilibrium is reached. By enhancing the concentration, leaving the adsorbent loaded from the measurement before, equilibrium points at higher concentrations can be determined. Thus, an adsorption isotherm can be constructed with sufficient equilibrium fluid phase concentration- uptake amount data. The amount of adsorbed substance (uptake) is calculated from the so called breakthrough curves. To demonstrate the calculation of the amount of adsorbed substances, the breakthrough profile of a single component adsorption system is presented in Figure 2.6. The figure shows a typical breakthrough profile of a system consisting of the adsorbent (the solid phase), the supercritical fluid

(the fluid phase) and the substance A (adsorbate). In the diagram, x axis represents the time and y axis represents the dimensionless concentration given by the ratio of the outlet concentration to the inlet (initial) concentration (C/C_0).The adsorbed amount of A on the substrate is given by the area I .

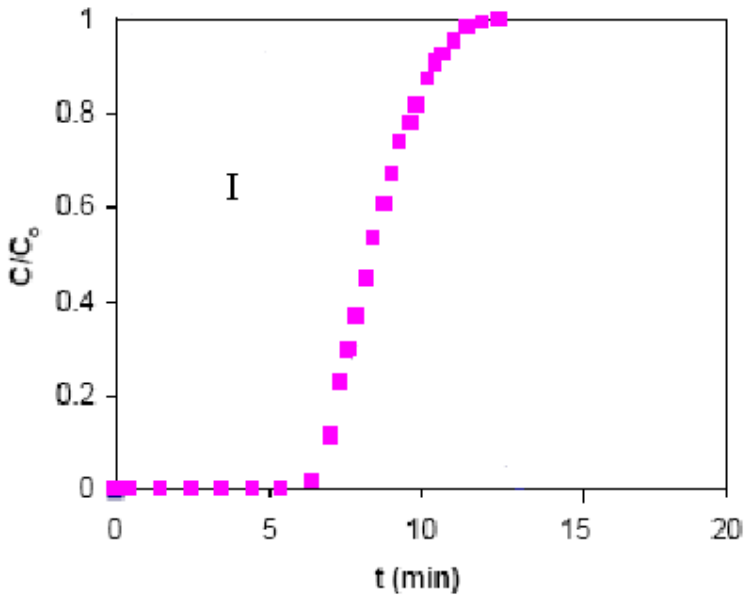

Figure 2.6: Breakthrough profile of a single component adsorption system

Erkey et al. determined the adsorption isotherms for naphtelene, phenanthrene, haxachlorobenzene and pentachlorophenol on soil using an experimental setup based on the principles of frontal analysis chromatography [29]. The adsorption isotherms were modeled based on Freundlich isotherm. For naphtelene, phenanthrene and hexachlorobenzene a linear adsorption isotherm was observed, wheras for pentachlorophenol a slight deviation from linearity was observed. Erkey et al. also measured adsorption isotherms for the same organics on carbon using the same technique [30]. In a study by Subra et. al., the adsorption of a mixture of thirteen terpenes from supercritical carbon dioxide on silanized silica was investigated [32].

From the breakthrough curves of the terpenes, they have seen that the adsorption of the terpenes on the silanized silica was competitive. The single component adsorption isotherms were represented by Langmuir like empirical equations due to the complex behaviour of the adsorption. They concluded that, multicomponent adsorption isotherms can be derived by again Langmuir like equations by regressing the constants using the experimental Another study was conducted by Harikrishnan et al to determine the adsorption isotherms of ethyl benzene on activated carbon using the breakthrough curves [33]. They looked at the effect of temperature and the pressure on the behaviour of the adsorption isotherms. The adsorption isotherm of ethyl benzene- activated carbon- $scCO_2$ system was represented by Langmuir isotherm. The adsorption of furfural and ethylacetate on activated carbon from $scCO_2$ was studied by Lucas et al. [34]. Again using the technique based on the frontal analysis chromatography, they measured adsorption isotherms at different temperatures and pressures. Three different adsorption isotherm models Langmuir, Freundlich and Redlich-Peterson were used in order to fit the experimental data. It was found that the best fit was obtained by Freundlich equation. They showed that the temperature has a direct effect on the adsorption capacity i.e. as the temperature increases, the adsorbed amount increases. More recently, Xing et al used the technique of breakthrough curves in order to determine the adsorption equilibria of artemisinin on silica aerogel from $scCO_2$ [35]. They used Freundlich adsorption isotherm model to correlate the data. Adsorption of CO_2 on the silica gel was also investigated and it was concluded that, the CO_2 was also adsorbing on the support which is referred to as the competitive adsorption of the CO_2 and artemisinin on the silica aerogel.

2.2.4.1.2. Determination of the Adsorption Isotherms by Perturbation Method

Perturbation chromatography is another method to investigate the single component and also multi component adsorption in a fluid system. Similar to the frontal analysis chromatography, perturbation chromatography is a continuous method where a mobile

phase is passed through the stationary phase and the analysis is done by a UV detector. Perturbation chromatography is also known as Minor Disturbance Method, Step and Pulse Method, Perturbation Method, Concentration Pulse Chromatography and Impulse Response Chromatography.

In Perturbation chromatography, a certain concentration of the component to be analyzed is fed into the stationary phase where the adsorbent is filled. The feed of the fluid phase is continued to be feed until adsorption equilibrium is reached. Then, the equilibrium is perturbed by injecting a small sample with differing concentration and the perturbance is analyzed by the response of the UV peak. Retention times of the peaks are recorded. In Figure 2.7 the perturbation chromatography of a two component system is given.

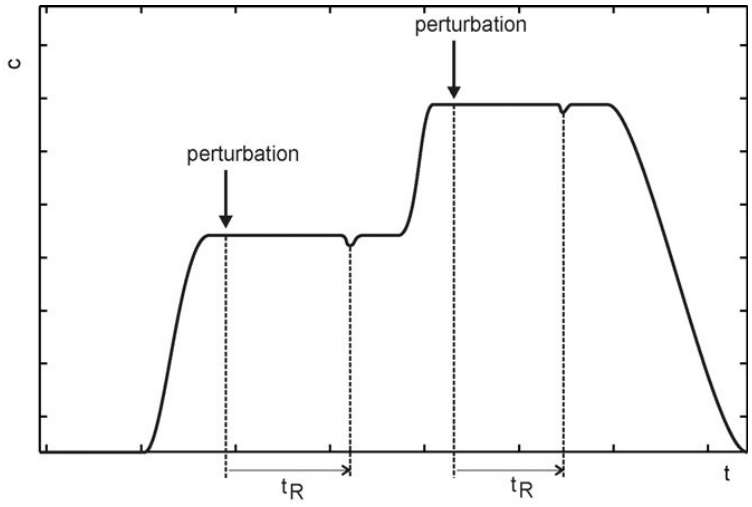

Figure 2.7: The Perturbation Chromatography profile for a two component system [26]

The adsorption isotherm slope is determined by using the retention times, then a set of differential equations are derived and solved to collect the adsorption data [36]. Using perturbation experiments Lübbert et al. investigated the adsorption of α and δ tocopherol on silica from mixtures of carbon dioxide and 2-propanol [36]. They

determined isotherms for both single and binary adsorption systems. Hill adsorption isotherm model which is an anti-Langmuir type model was used to correlate the data. Hill isotherm represented successfully the adsorption of both α and δ tocopherol on two silica supports Nucleosil and Kromasil. The effect of pressure was tested on the behaviour of the adsorption isotherm. It was seen that the adsorption amount decreased with increasing pressure, which was explained by higher solvent strength and density of the solvent (CO_2) at higher pressures.

2.2.4.1.3. Determination of the adsorption isotherms by elution by Characteristic point (ECP) Method

In this method, a certain amount of adsorbate sample is injected into the adsorbent which is placed in a chromatographic column and a chromatogram and a diffusion profile is obtained by elusion as shown in Figure 2.8. It is assumed that the adsorption equilibrium is reached. As it is seen from the figure at a characteristic point i the concentration in the fluid phase is C_i and q_i is given by the below equation.

$$q_i = \frac{1}{M}\int_0^{C_i} V_R(C)dC \tag{2.12}$$

$$V_R = V_i - V_0 \tag{2.13}$$

where M is the mass of adsorbent in the column; V_i is the retention volume of the characteristic point i and V_0 is the dead volume of the column.

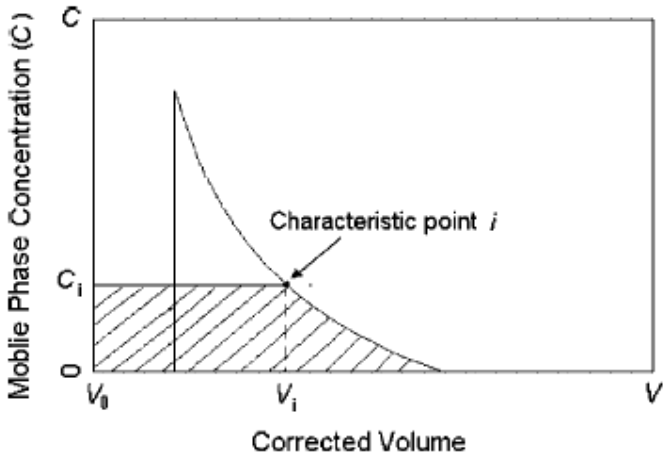

Figure 2.8: Chromatogram of elution by characteristic point method [37]

Using this method, if sufficient high concentrations are injected, each peak contains the whole information on the adsorption isotherm, thus an adsorption isotherm can be derived from a single peak. This method is fast, simple and can be used for pure substances.

Using the ECP method, Peper et al. determined the adsorption isotherms for the ibuprofen-enantiomers on a chiral modified silica gel Kromasil KR100-10-CHI-TBB [38]. In another study by Han et al., the adsorption isotherms of cis-5,8,11,14,17-eicosapentaenoic acid ethyl ester (EPA-EE) and cis-4,7,10,13,16,19-docosahexaenoic acid ethyl ester (DHA-EE) from $scCO_2$ on silica gel were measured [37]. The adsorption isotherm could best be represented by Langmuir model and it was also seen that the adsorption capacities of the two adsorbates were similar.

2.2.4.2. Static Methods

Even though dynamic methods to measure adsorption isotherms are easy and fast, these methods are not very suitable for the adsorption of precious organometallics on the porous supports. Because, in continuous measurements, a certain amount of solution

is passed through the system continuously and that leads to a big loss of the precursor. Moreover, the dynamic experimental set ups include large volumes of adsorbent columns which is not the requirement in this study. These methods are usually applied for industrial applications.

However, there are not many studies so far for the determination of the adsorption isotherms in supercritical fluid-solid systems with static methods where batch experimental techniques are applied. In a study by Smirnova et al., the adsorption of naphthalene and two drugs ketoprofene and miconazole on silica aerogels from $scCO_2$ was investigated [39]. The adsorption isotherms were measured for the two different systems and represented by Langmuir isotherm model. In another study by Zhang et al., the adsorption isotherm of bis (2,2,6,6-tetramethyl-3,5-heptanedionato) (1,5-cyclooctadiene) ruthenium (II) ($Ru(cod)(tmhd)_2$)- $scCO_2$- carbon aerogel system was measured by using a static experimental method [21]. The adsorption isotherm was again fitted to Langmuir isotherm. In a study by Erkey's group, the adsorption isotherms of platinum dimethyl cyclooctadiene ($PtMe_2COD$) on carbon aerogels were investigated. The isotherm was represented by Langmuir model [22]. For the studies mentioned above, the adsorbed amount of the precursors on the supports was found by using the weight increase of the support after fluid phase was removed by depressurizing. Then, the fluid phase concentration was obtained from the difference between the precursor put into the system initially and adsorbed by the substrate.

The adsorption of hydroxybenzoic asid on PMMA from $scCO_2$ was investigated by Diankov et al [28]. They fitted their experimental data to four different types of isotherms Langmuir, Freundlich, Sips and Toth isotherms. It was concluded that, Langmuir, Freundlich and Sips isotherms could not represent the data satisfactorily especially in the low and high limits of the isotherms. The adsorption isotherms were best represented by Toth Model. More recently, Aschenbrenner et al. investigated the adsorption $PtMe_2COD$ on two different supports silica gel and cordierite [23]. They measured the adsorption isotherms by developing a new experimental setup where a solution of $PtMe_2COD$ in $scCO_2$ was circulated over the supports in a closed system.

Then, they analyzed the fluid phase by using UV spectroscopy, and the uptake was determined from the difference of initial amount of $PtMe_2COD$ placed in the system and the amount of $PtMe_2COD$ in the fluid phase.

In this thesis, the adsorption isotherm of $PtMe_2COD$- $scCO_2$- RFA8 system was measured by developing an experimental setup where the fluid phase concentration could be measured. By knowing the concentration of the $PtMe_2COD$ in the fluid phase, the uptake was derived from the mass balance.

2.3. Kinetics of Adsorption

Kinetics of adsorption can generally be quantified by two different types of approaches. In the first approach, there are approximate equations which can be solved easily and also can be used to understand the controlling phenomena in the adsorption process. These models such as pseudo-first order, pseudo-second order and intraparticle diffusion models have been utilized frequently for a wide variety of systems [40, 41, 42]. However, these models are empirical and they are not very fundamental to describe the kinetics of adsorption of organometallics on the porous supports from supercritical solutions. They are mostly used for environmental applications, i.e. for the removal of organic contaminants from waste water. In the second approach, the different steps in the adsorption process are described using partial differential equations. This approach is the most vigorous and fundamental one in order to describe the kinetics of adsorption. However, there are very few studies on the investigation of kinetics of adsorption of a metal precursor on a porous support in supercritical CO_2. The first study was done by Zhang et al. which the kinetics of adsorption of a ruthenium precursor on carbon aerogel from $scCO_2$ was investigated by developing a kinetic model [21]. In another study by Aschenbrenner et al., the adsorption kinetics data were obtained for the adsorption of $PtMe_2COD$ on the two supports silica aerogel and monolithic cordierite [23]. Even though these two studies describe the kinetics of adsorption, they suffer from drawbacks in their experimental methods. In the study of Zhang et al, a batch

experimental technique was used to obtain fluid phase concentration-time data. They measured the adsorbed amount from the weight change of the support after removal of the $scCO_2$ and then calculated the fluid phase concentration from the mass balance. However, using this technique, the system has to be depressurized and restarted every time to get only one data point. Moreover, depressurization of the system may lead to some inaccuracies in the calculation of the uptake amount, for example the precursor may desorb from the adsorbent or the precursor can be lost to the atmosphere during the depressurization of the supercritical phase. In the study of Aschenbrenner et al., instead of measuring the adsorbed amount from the weight change after the depressurization of the system, they developed an experimental technique to analyze the fluid phase. Thus they obtained fluid phase concentration- time data in a unique adsorption experiment. The fluid phase concentration was determined by UV spectroscopy as a function of time and the uptake was determined from the difference of initial amount of precursor placed in the system and the amount of precursor in the fluid phase. However, accurate determination of uptake at longer times was not possible due to a drift in the baseline signal of the detector.

In this thesis, the adsorption kinetics data of $PtMe_2COD$-RFA8-$scCO_2$ system were obtained from a newly developed experimental technique, the fluid phase was analyzed using HPLC. Using this new technique, it was possible to get the concentration-time data without depressurization of the system and accurate results could be obtained from HPLC.

Chapter 3

Experimental Section

3.1. Materials

Resorcinol (99 %) and sodium carbonate (99.99 %) was purchased from Merck. Formaldehyde (36 %) was purchased from Lachema. $PtMe_2COD$ (99 % purity appears as white powder) was purchased from STREM chemicals, Inc. and ethanol (99.9 % purity) was purchased from Merck. The chemicals were used as received. Water was distilled and deionized. Carbon dioxide (99.998 %) and Nitrogen was purchased from Messer Aligaz.

3.2. Experimental Methods

3.2.1. Synthesis and Characterization of Resorcinol-Formaldehyde Aerogels (RFA)

3.2.1.1. Synthesis of the RFA8

Resorcinol-formaldehyde aerogels with a 8 nm average pore diameter (RFA8) were prepared by the polymerization reaction of resorcinol with formaldehyde in water with sodium carbonate as catalyst based on the procedure given by Pekala [43]. Figure 3.1 gives the various steps involved in the preparation and synthesis of RFA8 using the sol-gel method. In a typical procedure, a mixture of 1.2234 g resorcinol, 1.8535 ml formaldehyde, 5 ml distilled water and 0.0118 g sodium bicarbonate was prepared. The mixture was put in a glass tube or in spherical shaped glass molds. The mixtures in

glass tubes and spherical molds were sealed and kept at room temperature for one day, at 50°C for another day and at 90 °C for three successive days in an oven (Binder). The spherical and cylindrical gels (RF hydrogels or RF aquagels) were taken out of the glass molds and immersed in acetone for at least 12 hours in order to replace the unreacted reactants and water within the pores of the gels by the acetone.

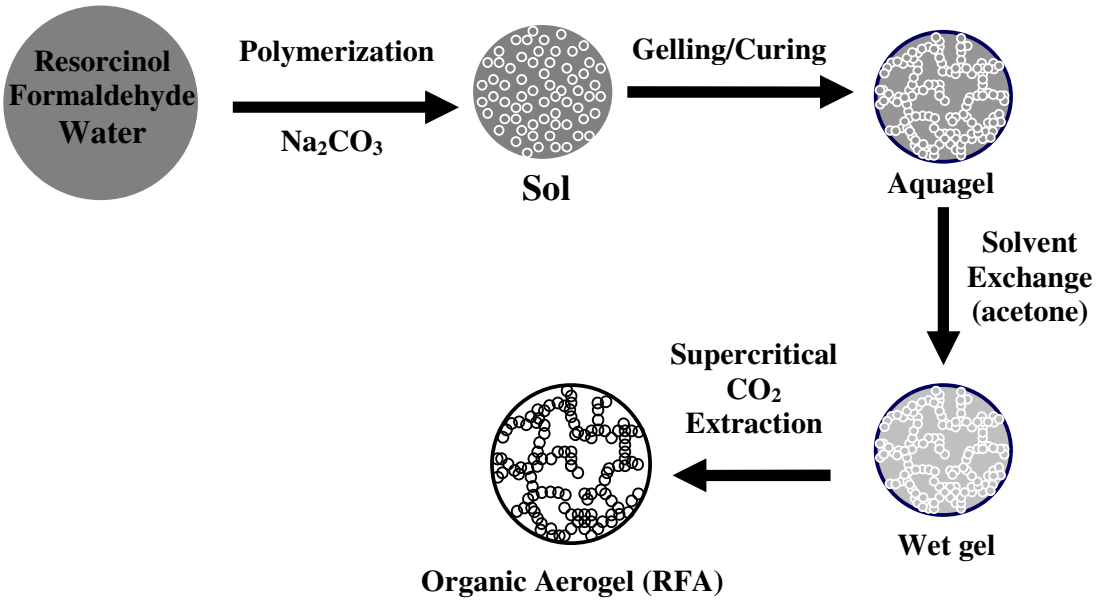

Figure 3.1: The procedure in the preparation and synthesis of resorcinol-formaldehyde aerogel using the sol-gel method.

3.2.1.2. Supercritical CO_2 Extraction of the RFA

For the drying of RF hydrogels, the supercritical CO_2 extraction method was used. The supercritical drying setup is given in Figure 3.2. The vessel used for the extraction experiments was custom manufactured from stainless steel and has an internal volume of 54 ml. It is equipped with two sapphire windows (2.5 cm in diameter, Sapphire Engineering, Inc., Pocasset; MA) and sealed with poly (ether ether ketone) o-rings. A thermocouple assembly (Omega Engineering, Inc.), a pressure transducer (Omega Engineering, Inc.) and a rupture disk assembly (Autoclave Engineers) are also attached to the vessel. For each extraction experiment, the vessel was first filled with acetone to avoid the evaporation of acetone within the pores of the wet gels. Then, the wet gels were placed inside the vessel together with a teflon coated stirring bar. A stainless steel screen was also included inside the vessel in order to separate the gels and the stirring bar. At room temperature, the system was pressurized with CO_2 up to 13.79 MPa using a syringe pump (Teledyne Isco, Model 260 D). The flow rate of CO_2 was kept constant at 150 ml/h by controlling it with a heated needle valve. The system was kept at these conditions until the acetone was displaced completely with CO_2. In order to understand that the acetone was displaced completely, the transformation of two phase system (CO_2+acetone) to a single phase system (CO_2) was observed, and also there was no liquid phase in the effluent anymore. Then, the system was heated to 50°C by a circulating heater/cooler (Cole Parmer, Model 12108-15), the flow rate was kept constant at 150 ml/h. The sufficient time for extraction of the acetone from the wet gel was determined by trying different extraction times. The selection criteria of the extraction time was the consistency of the textural and pore properties of the RFAs obtained since the presence of acetone and its eventual evaporation leads to a pore collapse. The synthesized aerogels were obtained in three different spherical, monolithic and crushed forms which are represented in Figure 3.3

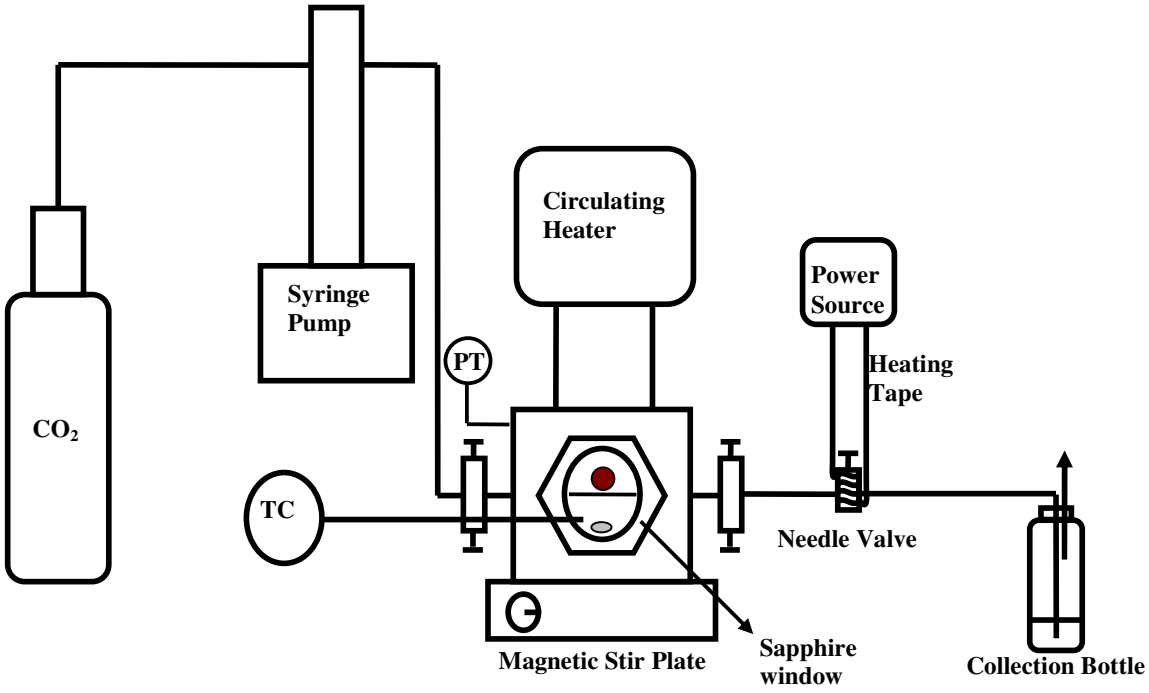

Figure 3.2: Schematic diagram of the extraction setup.

(a) (b) (c)

Figure 3.3: Three different forms of RFA8 (a) monolithic (b) crushed particles (c) spherical

3.2.1.3. Characterization

3.2.1.3.1. Linear Dimensions and Density Measurements

The dimensions (i.e. diameter, height) of the spherical and monolithic RFA8s were measured by using a caliper. The densities of the spherical aerogels and monolithic aerogels were derived from the measured mass and calculated volume. The crushed RFA8 particles were obtained by crushing the monoliths.

3.2.1.3.2. N_2 Physisorption Measurement

The surface area, total pore volume and pore size distribution of the synthesized RFA8 were determined from N_2 physisorption analysis by using a Micromeritics ASAP 2020 instrument.

Before starting the adsorption/desorption measurements, the RFA8 was degassed for 5 hours at 200 °C in order to remove any gas or impurities left inside the pores and surface of the aerogel. The surface area of RFA8 was found by using Branauer, Emmett and Teller (BET) equation. The BET surface area of the synthesized RFA8 was found as 759 m^2/g. The total pore volume of RFA8 was found as 2.45 m^3/kg. Total pore size distribution and average pore diameter were determined using the Barrett, Joyner and Halenda (BJH) method. Figure 3.4 represents the total pore size distribution of RFA8. As it can be seen in the figure, RFA8 is considered as a mesoporous substance since it contains mostly mesopores (pore sizes between 2-50 nm).

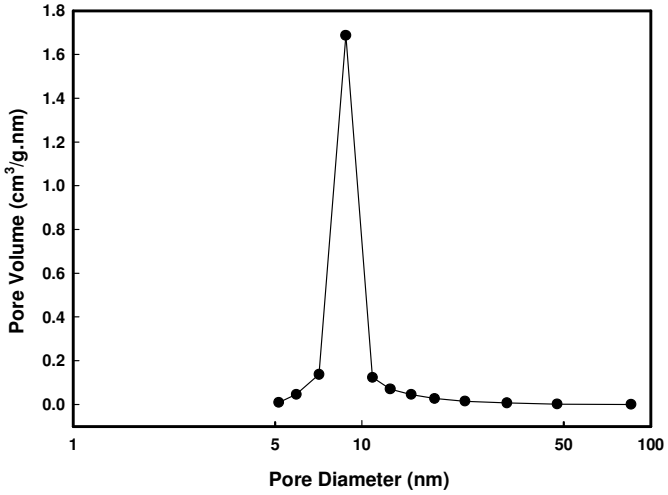

Figure 3.4: Pore Size Distribution of RFA8

3.2.2. Thermodynamics and Kinetics of Adsorption of $PtMe_2COD$ on RFA8 by supercritical CO_2 ($scCO_2$) Deposition Method

3.2.2.1. Adsorption isotherm experiments of $PtMe_2COD$ on RFA8 in $scCO_2$

A schematic diagram of the setup is given in Figure 3.6. The main components of the setup were those used in supercritical drying of the RFA8. For adsorption isotherm experiments, RFA8 was used in its crushed form. Crushed RFA8 particles were obtained by crushing the monolithic RFA8s into small particles. For each run, a certain amount of $PtMe_2COD$ and crushed RFA8 were placed in the vessel together with a stirring bar. Then, the vessel was heated to the desired temperature by a circulating heater/cooler. Subsequently, the vessel was pressurized quickly with CO_2 from the syringe pump up to the desired pressure. The stirrer (ARE heating magnetic stirrer,

VELP Scientifica) was started and set at a rotational velocity of 500 rpm. At a particular time, a small volume of the solution in the vessel was transferred and trapped in a sample loop by opening and closing the three-way valve (7). Subsequently, the sample loop was depressurized slowly by opening (9). The CO_2 was bubbled through an ethanol solution before being vented into the hood to trap any $PtMe_2COD$ that may be in the gas stream. Then, the loop was flushed with ethanol using a peristaltic pump (Gilson, Model Minipuls 3) in order to collect $PtMe_2COD$ that precipitated during depressurization. In order to determine the sufficient amount of ethanol needed to dissolve all the $PtMe_2COD$ in the loop, the loop was flushed successively with approximately 5 ml solutions of ethanol. The solutions were collected in vials and analyzed in HPLC. About 15 ml of ethanol was sufficient to dissolve all the $PtMe_2COD$ since no $PtMe_2COD$ could be detected in additional washes. After each sampling, the vessel was charged with CO_2 to the original pressure to compensate for the pressure drop that occurred during sampling. In order to empty the sample loop for the next sample, the ethanol left in the sample loop was removed by passing N_2 through the loop. At each particular time, this procedure was carried out twice in order to first remove the sample left in the short tube between the three-way valve (7) and the vessel during the previous sampling.

The samples were analyzed using High Performance Liquid Chromatography (HPLC) (Agilent Technologies, 1200 Series). In the analysis, 100 % ethanol with a flow rate of 1 ml/min was used as the mobile phase and the wavelength of the UV lamp of the detector was set to 220 nm. This wavelength was selected based on the UV spectra of a $PtMe_2COD$ in ethanol solution with a mass fraction of 100 ppm $PtMe_2COD$/ethanol. A series of $PtMe_2COD$-ethanol solutions with mass fractions ranging from (0 to 100 ppm) were used as the calibration solutions. Three different calibration curves were prepared since the relation between the concentration and area changes with different intervals of concentrations. Figure 3.5 shows the calibration curves for 0 to1 ppm, 1 to 5 ppm and 5 to 100 ppm $PtMe_2COD$-ethanol solutions.

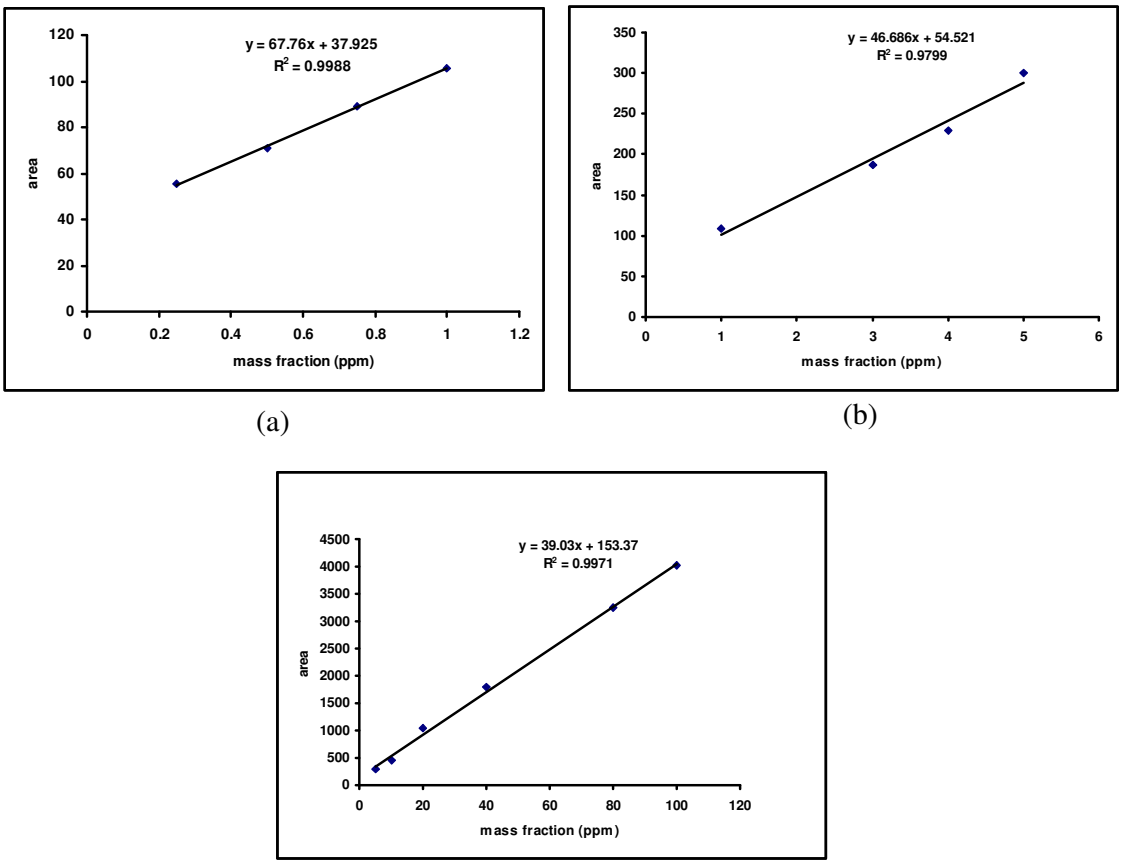

Figure 3.5: Calibration curves for (a) 0 to 1 ppm $PtMe_2COD$- ethanol solutions (b) 1 to 5 ppm $PtMe_2COD$- ethanol solutions (c) 5 to 100 ppm $PtMe_2COD$- ethanol solutions

In order to determine the volume of the sample loop, the two valves (7 and 9) and the loop were first weighed using an analytical balance (Adventurer Pro, AV 4101). Subsequently, the loop was filled with ethanol and the two valves and the filled loop were weighed once more. The weight of ethanol in the loop was determined from the weight difference and was converted to the volume of the loop using the density of

ethanol at room temperature (789 kg/m^3). This procedure was applied three times in order to determine the accuracy of the calculation of the volume of the sample loop. The loop volume was determined as 0.16 ml with an accuracy of ± 0.01 ml.

In order to determine the fluid phase concentration and uptake of $PtMe_2COD$ at a particular sampling time, the following calculation procedure was followed.

First, the amount of $PtMe_2COD$ (kg) in the sample loop for the ith sample at time t, $(m_{SL})_i$, was determined by:

$$(m_{SL})_i = (m_{et})_i \times C_{HPLC} \tag{3.1}$$

where $(m_{et})_i$ is the amount of ethanol (kg) that was used to dissolve the $PtMe_2COD$ which precipitated in the sample loop and C_{HPLC} is the concentration (kg $PtMe_2COD$/kg ethanol) of the ethanol+ $PtMe_2COD$ solution which was obtained using HPLC. Then, the amount of CO_2 (kg) in the sample loop, $(m_{CO_2})_{SL}$, was calculated by:

$$(m_{CO_2})_{SL} = V_{SL} \times \rho_{CO_2} \tag{3.2}$$

where V_{SL} is the volume of the sample loop and ρ_{CO_2} is the density of CO_2 in the sample loop.

Using the amount of $PtMe_2COD$ and the amount of CO_2 in the sample loop, the mass fraction in the sample loop (kg $PtMe_2COD$/ kg CO_2) for the ith sample, $(w_{SL})_i$, was obtained by the equation:

$$(w_{SL})_i = \frac{(m_{SL})_i}{(m_{CO_2})_{SL}} \tag{3.3}$$

Since mass fraction in the sample loop is equal to the mass fraction in the vessel at time t, the following equality holds for the mass fraction in the vessel:

$$(w_{SL})_i = (w_{vessel})_i \tag{3.4}$$

Therefore, the fluid phase concentration in the vessel (mole $PtMe_2COD$/kg CO_2) at time t, C_i, is given by:

$$C_i = \frac{(w_{vessel})_i}{MW_{PtMe_2COD}} \tag{3.5}$$

where $MW_{PtMe2COD}$ is the molecular weight of $PtMe_2COD$ (333.3 g/moles).

In order to determine the adsorption isotherms, it is necessary to ensure that the system has reached equilibrium. Therefore, two or three samples were taken for the determination of the equilibrium concentration of the fluid phase. When the last two fluid phase concentrations were equal, the sampling was stopped. In order to calculate the uptake concentration of $PtMe_2COD$ by the RFA8 (mol $PtMe_2COD$/kg RFA8) at equilibrium the following equation was used.

$$q = \frac{m_{initial} - \sum_{k=0}^{i-1}(m_{SL})_k - (m_{vessel})_i}{m_{RFA8} \times MW_{PtMe_2COD}} \tag{3.6}$$

where $m_{initial}$ is the amount of $PtMe_2COD$ that was placed in the vessel (kg) at the beginning of the experiment and m_{RFA8} is the amount of RFA8 (kg) that was placed in the vessel. $(m_{vessel})_i$ is the amount of $PtMe_2COD$ (kg) in the vessel at t=t when the i^{th} sample was taken and it was calculated with the following equation:

$$(m_{vessel})_i = (w_{vessel})_i \times (m_{CO_2})_{vessel} \tag{3.7}$$

where $(m_{CO2})_{vessel}$ is the amount of CO_2 in the vessel which was calculated by multiplying the volume of the vessel and the density of CO_2 in the vessel. In Equation

(3.6), the summation term accounts for the cumulative amount of $PtMe_2COD$ removed from the vessel when the previous samples were taken.

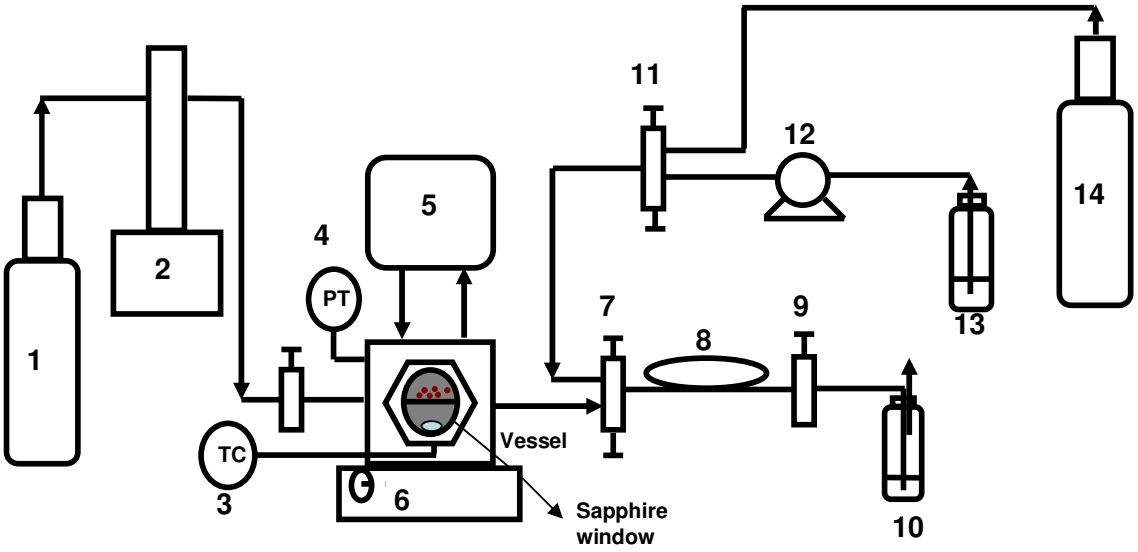

1.CO_2 Cylinder 2. Syringe Pump 3. Thermocouple Assembly 4. Pressure Transducer 5. Circulating Heater 6. Magnetic Stirrer 7. Two-way Valve 8. Sample loop 9. One-way valve 10. Collection Vial 11. Two-way valve 12. Peristaltic pump 13. Ethanol reservoir 14. N_2 Cylinder

Figure 3.6: Schematic Diagram of the Adsorption Isotherm Experiment Setup

3.2.2.2. Adsorption kinetics experiments of $PtMe_2COD$ on RFA8 in $scCO_2$

In order to obtain the adsorption kinetics data of $PtMe_2COD$ on RFA8 in $scCO_2$, the same procedure in the adsorption isotherm experiments was followed. In these experiments RFA8s were used in their spherical forms. For each run a spherical RFA8 and a certain amount of $PtMe_2COD$ was placed in the vessel. At particular times, the samples were taken from the fluid phase and the fluid phase concentrations were calculated from the equations represented above. The fluid phase concentrations (mol $PtMe_2COD/m^3$ $scCO_2$) versus time data was collected for three spherical RFA8s with changing diameters.

This experimental technique enables us to obtain data both on the kinetics and the thermodynamics of adsorption. An important issue is that a pressure drop occurs in the vessel each time a sample is taken. The pressure is restored to its original value by charging the system with CO_2 after taking each sample. However, adding fresh CO_2 to the system every time a sample is taken leads to a decrease in fluid phase concentration. In our experiments this error is negligible due to the small volume (0.16 ml) of the sample loop. This error further decreases in adsorption isotherm determination because, only two or three samples are taken during the experiment.

3.2.3. Reduction Experiments

After conducting the adsorption of $PtMe_2COD$ on RFA8, the adsorbed $PtMe_2COD$ was reduced to its metal form. First, a known amount of the prepared $PtMe_2COD$/RFA8 was placed in an alumina process tube and put into a tubular furnace (Thermolyne 21100). Before starting the reduction process, the air inside the furnace was removed to have an inert atmosphere under flowing N_2. Then, H_2 with a flow rate of 100 mL/min was passed through the furnace for 4 hours at 200°C. Later, H_2 was switched to N_2 and temperature was increased to 250°C in order to break H_2-Pt bonds. Then, the system was started to cool down to room temperature under flowing N_2 .The sample was then removed from the furnace and weighed. The Pt metal loading was determined from the weight decrease by using an analytical balance. For the characterization of the synthesized Pt/RFA8 particles, XRD continuous measurements were carried out by using Cu Kα source Huber G 670 Imaging Plate in a 2θ range of 5^0-86.915^0 with a scanning rate of $5.5^0\,min^{-1}$.

Chapter 4

Results and Discussion

4.1. Testing for the accuracy of the experimental setup

Before conducting measurements on the adsorption isotherm and adsorption kinetics, a set of experiments were carried out in order to test the accuracy of the concentration measurement using our sampling system. First, a known amount of $PtMe_2COD$ was placed inside the vessel. Then, CO_2 was charged to the system to the desired pressure using the syringe pump. After, the vessel was filled with CO_2, the system was heated to the desired temperature using the circulating heater. Then, four successive samples were taken from the system. These samples were analyzed in HPLC and measured concentrations of the samples were recorded and converted to the concentration in the sample loop using equation 3.3.

From the concentrations in the sample loop, the concentrations in the vessel were calculated. The measured concentrations were compared to the predicted concentrations in the vessel. Figure 4.1 shows the plot of predicted concentrations versus measured concentrations in the vessel. It can be seen that there was a good agreement between the concentrations in the vessel measured from the analysis of the samples and predicted concentrations in the vessel. The slight changes in the concentrations arise from the loss of the $PtMe_2COD$ that is lost by trapping it in the sample loop at each sampling. However, this concentration change is about 2 %, due to the small volume of the sample loop.

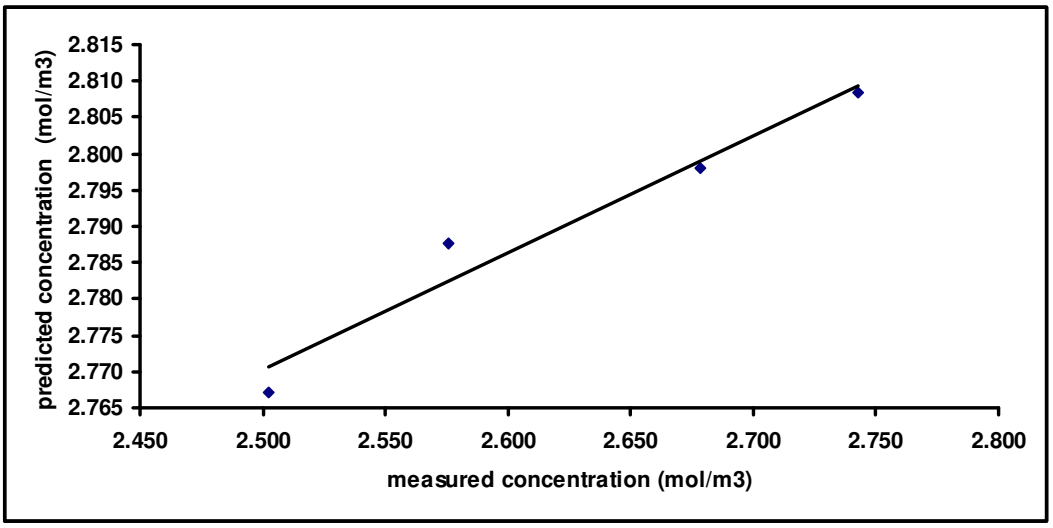

Figure 4.1: The test for the accuracy of the experimental set-up

4.2. Adsorption Isotherm of $PtMe_2COD$-RFA8-$scCO_2$ System

Adsorption isotherm of $PtMe_2COD$ on RFA8 in $scCO_2$ was measured at 20.7 MPa and 333 K. This isotherm gives the relation between the concentration of $PtMe_2COD$ in the fluid phase (mol $PtMe_2COD$/ m^3 $scCO_2$) and the uptake amount of $PtMe_2COD$ on the substrate (mol $PtMe_2COD$/kg RFA8) at the equilibrium of the system. Figure 4.2 shows the adsorption isotherm for $PtMe_2COD$-$scCO_2$- RFA8 system. As the figure indicates, at very low fluid phase concentrations the uptake amount increases very sharply. However, after a certain value of fluid phase concentration the uptake becomes constant. The experimental data was represented by two different adsorption isotherms, Langmuir and Freundlich isotherms. Langmuir model is one of the simplest and most useful models for description of both chemical and physical adsorption. It can be represented by equation 4.1.

$$q = \frac{K_1 Q_0 C}{1 + K_1 C} \tag{4.1}$$

where, q (mol/kg) is the uptake amount of the adsorbate ($PtMe_2COD$) on adsorbent (RFA8), K_1 is the Langmuir adsorption constant (m^3 $scCO_2$/mol $PtMe_2COD$) and Q_0 is the adsorption capacity (mole $PtMe_2COD$/ kg RFA8). C is the concentration of $PtMe_2COD$ in $scCO_2$ (mol/ m^3 $scCO_2$). K_1Q_0 is the relative affinity of the adsorbate towards the surface of the adsorbent. The constants in the model were found by nonlinear regression analysis as K_1= 310 m^3 $scCO_2$/mol $PtMe_2COD$ and Q_0=1.4 mole $PtMe_2COD$/ kg RFA8. Freundlich model was also used to fit the data. Freundlich model can be represented by the equation below.

$$q = K_f C^{1/n} \tag{4.2}$$

Where K_f is the Freundlich adsorption constant and n is the Freundlich exponent. The constants were found using nonlinear regression analysis.

The model fits are shown in Figure 4.2. The best fit to the experimental data was obtained by the Langmuir Model with a fitting error of 4 %. The fitting error of Freundlich model was found as 7 %. Therefore, the Langmuir model was used in the model that was developed to describe the kinetics of adsorption.

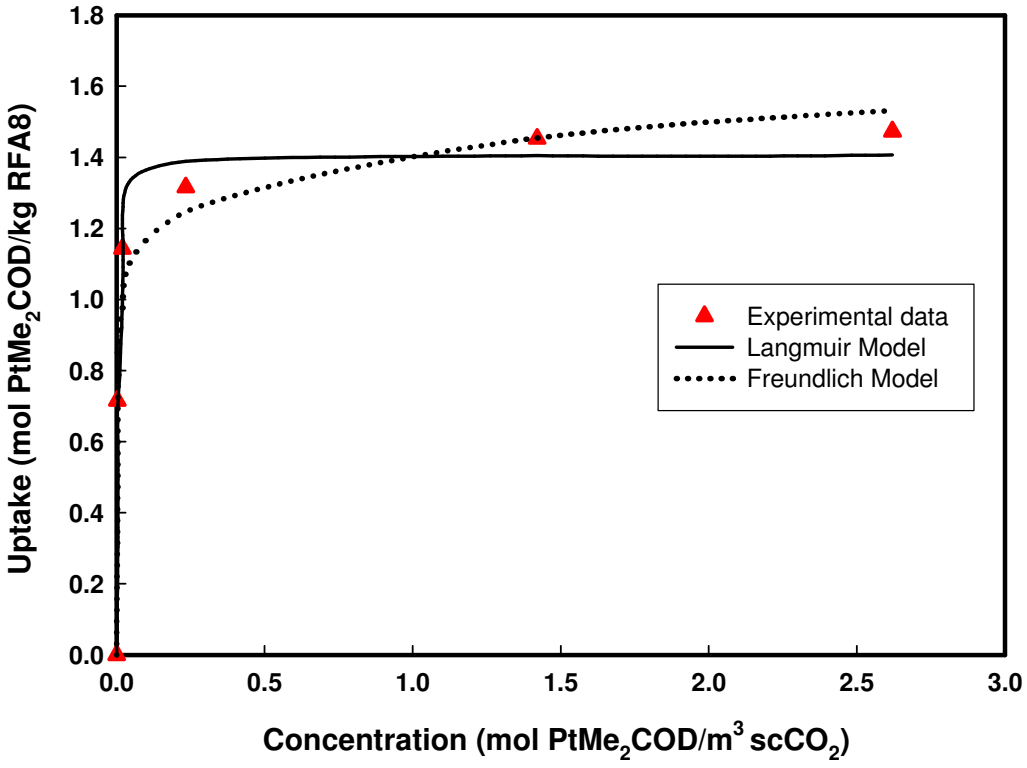

Figure 4.2: Adsorption isotherms for $PtMe_2COD$-$scCO_2$-RFA8 system at 20.7 MPa and 333 K

4.3. Adsorption Kinetics Model Development for $PtMe_2COD$-$scCO_2$-RFA8 System

In order to describe the kinetics of adsorption of $PtMe_2COD$ on RFA8 in $scCO_2$, a model was developed. In the model, diffusion of $PtMe_2COD$ through the pores of RFA8 and also adsorption on the surface of the pores of the RFA8 were taken into account. The adsorption process of $PtMe_2COD$ on RFA8 from $scCO_2$ can be described by four successive steps.

1. Mass transfer of $PtMe_2COD$ from $scCO_2$ to RFA8.

2. Diffusion of $PtMe_2COD$ (dissolved in $scCO_2$) in the pores of RFA8.
3. Adsorption of $PtMe_2COD$ on the surface of the pores of RFA8.
4. Surface diffusion within RFA8.

The first mass transfer step is best described by film diffusion which relates the flux N_A to the concentration difference between the bulk and the surface by a mass transfer coefficient (k_m).

$$N_A = k_m(C_{A,b} - C_{A,s}) \tag{4.3}$$

For our system, the concentrations of the bulk ($C_{A,b}$) and the surface ($C_{A,s}$) was considered as equal by assuming that there is no mass transfer resistance between the surface and the bulk. Therefore the first mass transfer step was neglected.

The second step which is the diffusion of $PtMe_2COD$ through the pores of spherical RFA8 particles in the radial direction is described by Fick's first law of diffusion which is given in equation 4.4.

$$N_A = -D_{e,p}\frac{\partial C_A}{\partial r} \tag{4.4}$$

where C_A is the concentration of $PtMe_2COD$ in pore volume and $D_{e,p}$ is the effective diffusion coefficient. Effective diffusion coefficient is a modified form of binary diffusion coefficient D_{AB} (A stands for $PtMe_2COD$ and B stands for $scCO_2$) which takes into account the porosity (ε_p) and tortuosity (τ) of the RFA8 and also a size restriction factor F (λ). Tortuosity can be adjusted varying from less than unity to more than 6 depending on experimental data [44]. Tortuosity is defined as the ratio of the actual distance of a molecule that travels between two molecules to the shortest distance between those two points [45]. The equation for effective diffusion coefficient is given below.

$$D_{e,p} = \frac{F(\lambda)\varepsilon_p D_{AB}}{\tau} \tag{4.5}$$

The size restriction factor F (λ) can be represented by equation 4.6 [46].

$$F(\lambda) = 1.03e^{-4.5\lambda} \tag{4.6}$$

where λ is the ratio of the critical diameter of the solute ($PtMe_2COD$) to the pore size of the adsorbent (RFA8). Critical diameter of $PtMe_2COD$ was found as 0.6 nm by using Marvin Beans software. The pore size of the RFA8 is 8 nm.

In order to estimate the binary diffusion coefficient D_{AB}, the Schmidt number correlation proposed by Funazukuri et al. was used [46]. The correlation is given by,

$$Sc^{+} = \frac{Sc}{Sc^{*}} = 1 + \exp\left[\sum_{i=0}^{5} a_i \left(\frac{\upsilon_0}{\upsilon}\right)^i\right] \tag{4.7}$$

For binary diffusion,

$$Sc^{*} = \frac{5}{6}\left[\frac{\sigma_1 + \sigma_2}{2\sigma_2}\right]^2 \left[\frac{2M_1}{M_1 + M_2}\right]^{1/2} \tag{4.8}$$

where Sc is the Schmidt number at high pressure and Sc* is the Schmidt number at atmospheric pressure. Sc^{+} is given by the ratio of the Schmidt number at high pressure to that at atmospheric pressure. σ_1 and σ_2 is the hard sphere diameters of $PtMe_2COD$ and CO_2 respectively (0.6 nm and 0.4 nm) . M_1 and M_2 are the molecular weights of the two molecules (333 g/mol and 44 g/mol). υ term in equation 4.7 stands for the molar volume of the solvent and υ_0 is the hard-sphere closest packed volume of the solvent molecules. υ_0 is related to temperature and given by equation (4.9) [46] ,

$$\upsilon_0 = \frac{1}{1.384}\left(\sum_{i=0}^{4} c_i T^i\right) \tag{4.9}$$

The constants "a_i" and "c_i" in equations 4.7 and 4.9 are given in table 4.1.

Table 4.1: Constants in correlation of Schmidt number with solvent molar volume (a_i) and effective hard-sphere packed volume (c_i) [46]

i	**a_i**	**c_i**
0	-4.92519817	4.452×10^{-5}
1	54.5529385	-1.152×10^{-7}
2	-245.231443	2.749×10^{-10}
3	607.893924	-3.073×10^{-13}
4	-708.884016	1.290×10^{-16}
5	329.611433	-

Sc^+ number was calculated from equation 4.6 and 4.8 by using constants "a_i" and "c_i" in Table 4.1 and molar volume of CO_2 (υ) which is 5.98×10^{-5} m^3/mol. Then, Sc* number was calculated from equation 4.8 by using σ_1, σ_2 and M_1, M_2 values. After determining Sc^+ and Sc* numbers, Sc number was calculated. In order to determine binary diffusion coefficient D_{AB}, equation 4.10 was used.

$$Sc = \frac{\nu}{\rho \times D_{AB}} \tag{4.10}$$

where, ν is the kinematic viscosity and ρ is the density of the $scCO_2$ at the system conditions.

For our system, the viscosity (ν) of $scCO_2$ at 20.7 MPa and 333K is 0.065 Cp and the density (ρ) of $scCO_2$ is 736.1 kg/m^3. Binary diffusion coefficient (D_{AB}) for $PtMe_2COD$-$scCO_2$ binary system was calculated as $1.32x10^{-8}$ m^2/s. Finally, the effective diffusion coefficient ($D_{e,p}$) was calculated from equation 4.4 by using F (λ), ε_p and τ values. The porosity value (ε_p) was calculated from the ratio of the total pore volume of the RFA8 to the volume of spherical RFA8. Tortuosity value (τ) was taken as the reciprocal of the ε_p. F (λ) was calculated from equation 4.5 as 0.735. Then, $D_{e,p}$ was calculated as $5.99x10^{-9}$ m^2/s.

The third step in the model which is the adsorption of $PtMe_2COD$ on the surface of RFA8 was identified through the adsorption isotherm of $PtMe_2COD$-$scCO_2$-RFA8 system which was shown in Figure 4.2.

The final step is the surface diffusion of the $PtMe_2COD$ within RFA8 meaning that, the solute adsorbed onto the surface of the adsorbent migrates along the surface under the concentration gradient in the adsorbed phase. However, this step was neglected since it was assumed that there is a strong adsorption bond between $PtMe_2COD$ and RFA8 molecules and therefore no surface diffusion occurred.

After investigating all the four steps, the kinetic model was developed by considering steps 2 and 3 which are the supercritical diffusion of $PtMe_2COD$ in the pores of RFA8 particles and adsorption of $PtMe_2COD$ on the surface of RFA8 particles.

For the derivation of the adsorption kinetics model, the unsteady state adsorption process was described by a partial differential equation which was obtained by deriving a spherical shell balance for the RFA8 particle. Figure 4.3 represents the mass transfer steps for diffusion of $PtMe_2COD$ into RFA8 particle and shell balance in spherical RFA8 particle.

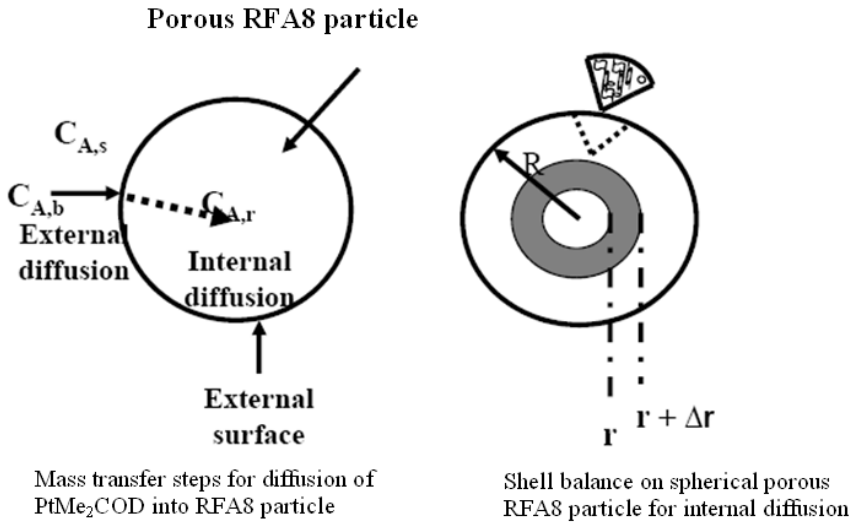

Figure 4.3: Representation of mass transfer steps and shell balance for diffusion $PtMe_2COD$ on RFA8

The partial differential equation derived from the spherical shell balance for the adsorption kinetics model is given in equation 4.11. The derivation of the equation is given in Appendix B.

$$\varepsilon_p \frac{\partial C_A}{\partial t} + \rho_p \frac{\partial q}{\partial t} = D_{e,p}\left(\frac{\partial^2 C_A}{\partial r^2} + \frac{2}{r}\frac{\partial C_A}{\partial r}\right) \tag{4.11}$$

where C_A is the concentration of $PtMe_2COD$ in $scCO_2$ (mol/m^3), q is the uptake concentration of $PtMe_2COD$ on RFA8 (mol/kg) and t is time (s). The term $\frac{\partial C_A}{\partial t}$ represents the accumulation term, $\frac{\partial q}{\partial t}$ represents the adsorption term and $\frac{\partial C_A}{\partial r}$ represents the flux term. The boundary conditions are;

Boundary Condition-1: $\frac{\partial C_A}{\partial r} = 0$ at r= 0

Boundary Condition-2: - V $\frac{\partial C_A}{\partial t} = m\ S\ D_e\ \frac{\partial C_A}{\partial r}$ at r= R

where, V is the volume of $scCO_2$ (high pressure vessel), m is the mass and S is the external surface area of RFA8 particles, respectively. The initial conditions for equation 4.10 are;

Initial Condition-1: $C_A = 0$ at t= 0 at $0 \le r < R$

Initial Condition-2: $C_A = C_{A0}$ at t= 0 at r= R

Equation 4.11 was modified by substituting the isotherm relation for the accumulation term and using the chain rule, the following equation was obtained;

$$\frac{\partial C_A}{\partial t} = \frac{D_e}{\varepsilon_p + \rho_p (\frac{\partial q}{\partial C_A})} (\frac{\partial^2 C_A}{\partial r^2} + \frac{2}{r}\frac{\partial C_A}{\partial r}) \tag{4.12}$$

The above equation was converted to a set of ordinary differential equations (ODEs) by using the numerical method of lines method (NMOL) as represented in equation 4.13.

$$\frac{dC_{A(n)}}{dt} = \frac{D_{e,p}}{\varepsilon_p + \rho_p (dq/dC_{A(n)})} \left(\frac{C_{A(n+1)} - 2C_{A(n)} + C_{A(n-1)}}{(\Delta r)^2} + \frac{2}{R-(n-1)\Delta r} \frac{C_{A(n-1)} - C_{A(n+1)}}{2\Delta r} \right) \tag{4.13}$$

And the boundary conditions were identified as,

$C_{A(n)} - C_{A(n-1)} = 0$ at r=0 (4.14)

$$\frac{dC_{A(1)}}{dt} = \frac{mSD_{e,p}}{-V} \frac{C_{A(1)} - C_{A(2)}}{\Delta r} \quad \text{at r=R} \tag{4.15}$$

Then, equation 4.13 with the boundary conditions was solved simultaneously in MATLAB by using ODE15s solver. The MATLAB program was given in Appendix A.1. n number in equation 4.13 denotes the number of points in the radial direction from the surface of the spherical RFA8 particle to the center of the particle. Different n values increasing from 25 to 3000 was tried in the model, and it was seen that after n=1000 the results of the model did no longer change. Therefore, 1000 increments through the radius were sufficient in the model to describe the adsorption kinetics.

Figure 4.4 represents the concentration values at different points through the radius with changing n values. As it can be seen in the figure with increasing n, the data becomes smoother, and it enables us to get more accurate results from the adsorption kinetics model.

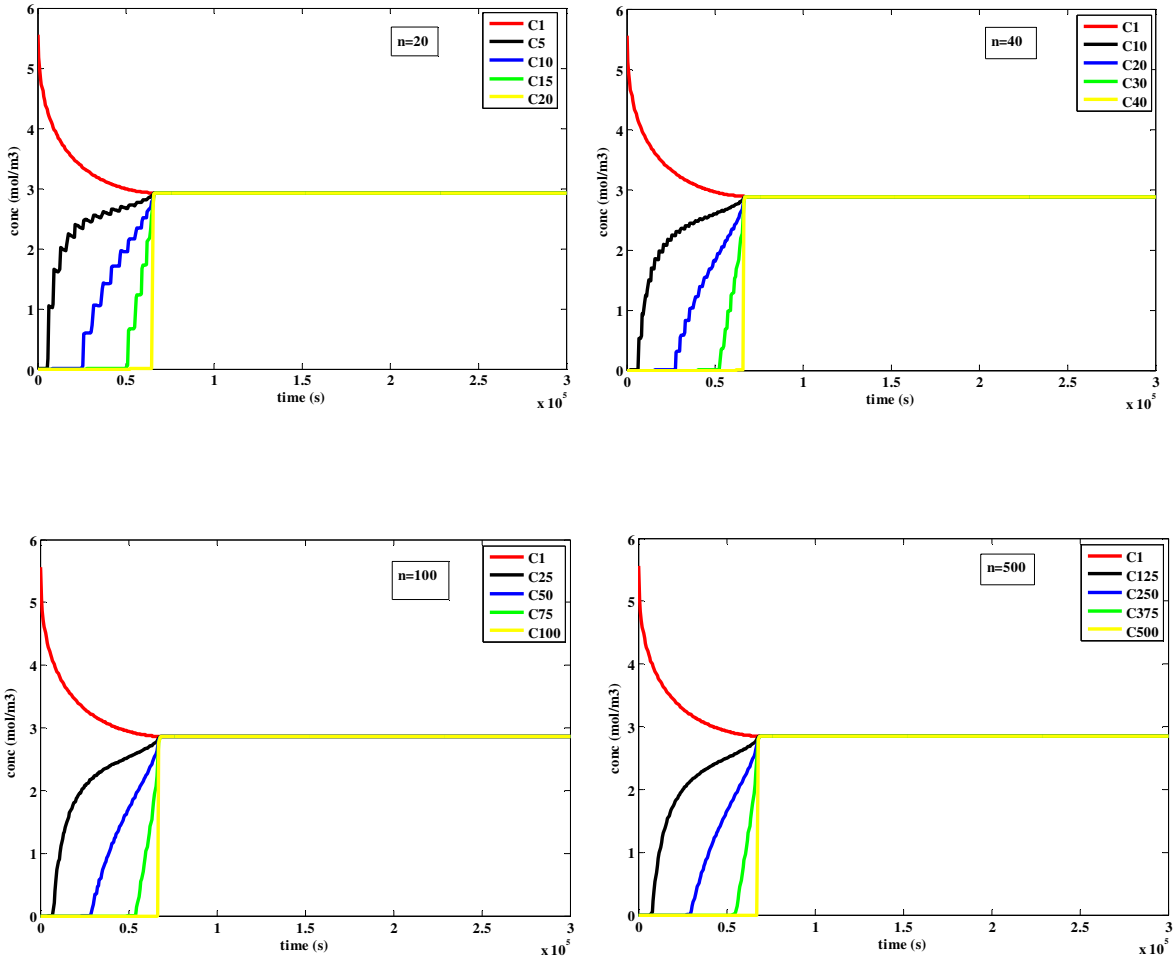

Figure 4.4: Effect of n to the model results

All the parameters used in the model were given in Table 4.2.

Table 4.2: Parameters used in the adsorption kinetics model

	Parameters	Definition	Unit	Value
Adsorbent (RFA8) Properties	ρ_p	Density	kg/m^3	342
	R_p	Radius of spherical RFA8 particles	m	0.003-0.005
	ε_p	Porosity	-	V_{tot}/V_{RFA8}
	M	Mass of RFA8 used in experiments	kg	$1x10^{-4}$, $1.5x10^{-4}$
	S	External surface area per mass of spherical RFA8 particles	m^2/kg	$3/(\rho_p R)$
	τ	Tortuosity- the adjustable parameter of the system	-	adjustable
Bulk $scCO_2$ properties	V	Volume of $scCO_2$ (Volume of high pressure vessel)	m^3	$54x10^{-6}$
	C_{A0}	Initial concentration of $PtMe_2COD$ in $scCO_2$ at t=0	mol/m^3	2.71, 2.78, 5.56
Isotherm Properties	K_1	Langmuir adsorption constant	m^3 $scCO_2$/mole $PtMe_2COD$	309.9564
	Q_0	Adsorption capacity	m^3 $scCO_2$/kg RFA8	1.4082
Transport Properties	D_{AB}	Binary diffusion coefficient	m^2/s	$1.32x10^{-8}$
	d_s	Solute molecule diameter	nm	0.6
	d_p	Pore diameter of RFA8	nm	8
	λ	d_s/d_p	-	0.075
	$F(\lambda)$	$1.03e^{-4.5\lambda}$	-	0.735
	$D_{e,p}$	Effective diffusion coefficient	m^2/s	$D_{e,p} = \frac{F(\lambda)\varepsilon_p D_{AB}}{\tau}$

The comparison of the model results with the experimental data is represented in Figures 4.5, 4.6 and 4.7. The average fitting error of the model to the experimental data is 7.2 %. The model was used for three different experiments which the volume of spherical RFA8 particles and the initial concentration of $PtMe_2COD$ in $scCO_2$ were changed. In all of the three experiments, adsorption kinetics data were measured at 20.7 MPa and 333 K. As it can be seen from the figures, the model results fit well with the experimental data. For all the three different experiments, the tortuosity value was kept constant as $1/\varepsilon_p$. Since there are no adjusted parameters in the model, the good agreement between the model and the data suggest that the model is accurate in describing the kinetics.

Figure 4.5 represents the adsorption kinetics data measured for an initial concentration of 2.78 mol $PtMe_2COD/m^3$ $scCO_2$ and a mass of 135 mg spherical RFA8 particle. Figure 4.6 represents the adsorption kinetics data for an initial concentration of 2.71 mol $PtMe_2COD/m^3$ $scCO_2$, but this time with a mass of 51.5 mg spherical RFA8 particle. As the figures 4.5 and 4.6 indicate, the equilibrium concentrations are not the same although the two experiments have close initial concentrations. The reason for this is the higher surface area of the first RFA8 particle since it has a larger mass. The total surface area of a RFA8 particle determines the amount of $PtMe_2COD$ molecules adsorbed on the surface of RFA8. Therefore, the equilibrium concentration in figure 4.5 is much lower than the equilibrium concentration in figure 4.6. In figure 4.5, almost all of the $PtMe_2COD$ molecules adsorbed on the surface of RFA8, however in figure 4.6 the system reached equilibrium before all the $PtMe_2COD$ molecules adsorbed on the surface.

In Figure 4.7, the adsorption kinetics data is shown for a 5.56 mol $PtMe_2COD/m^3$ $scCO_2$ initial concentration and a mass of 148.8 mg RFA8. The good agreement between the experimental data and the model results is also seen in this figure.

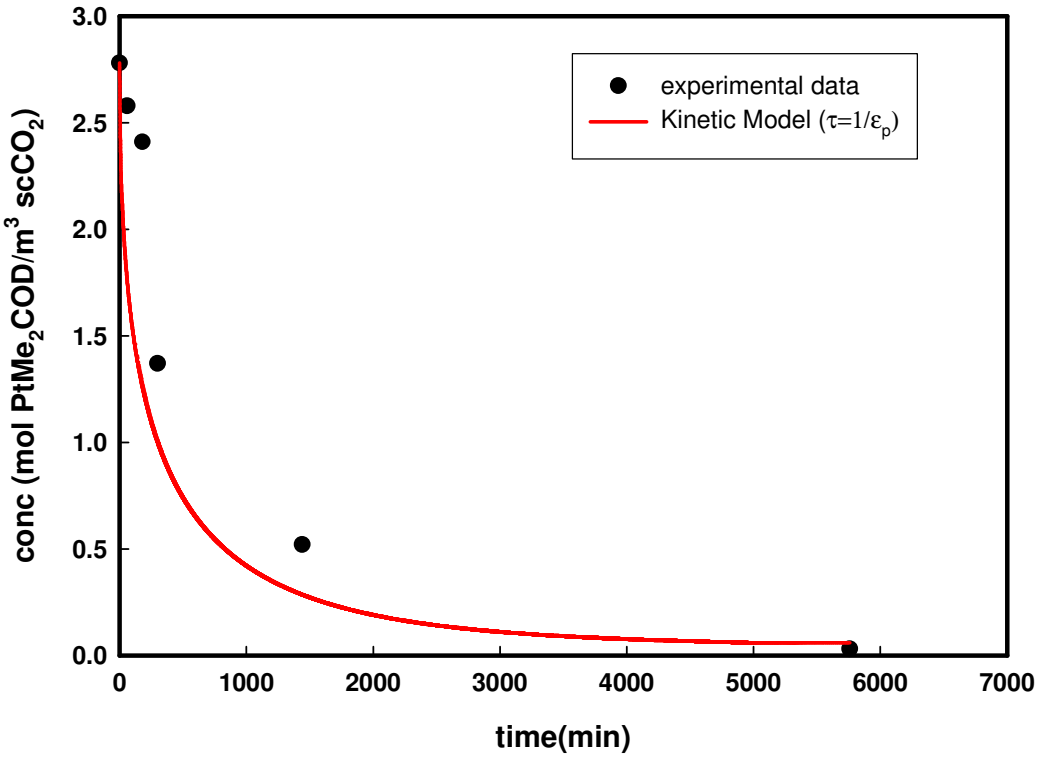

Figure 4.5: Experimental data and adsorption kinetics model,
Initial concentration= 2.78 mol $PtMe_2COD/m^3$ $scCO_2$, m_{RFA8}= 135 mg

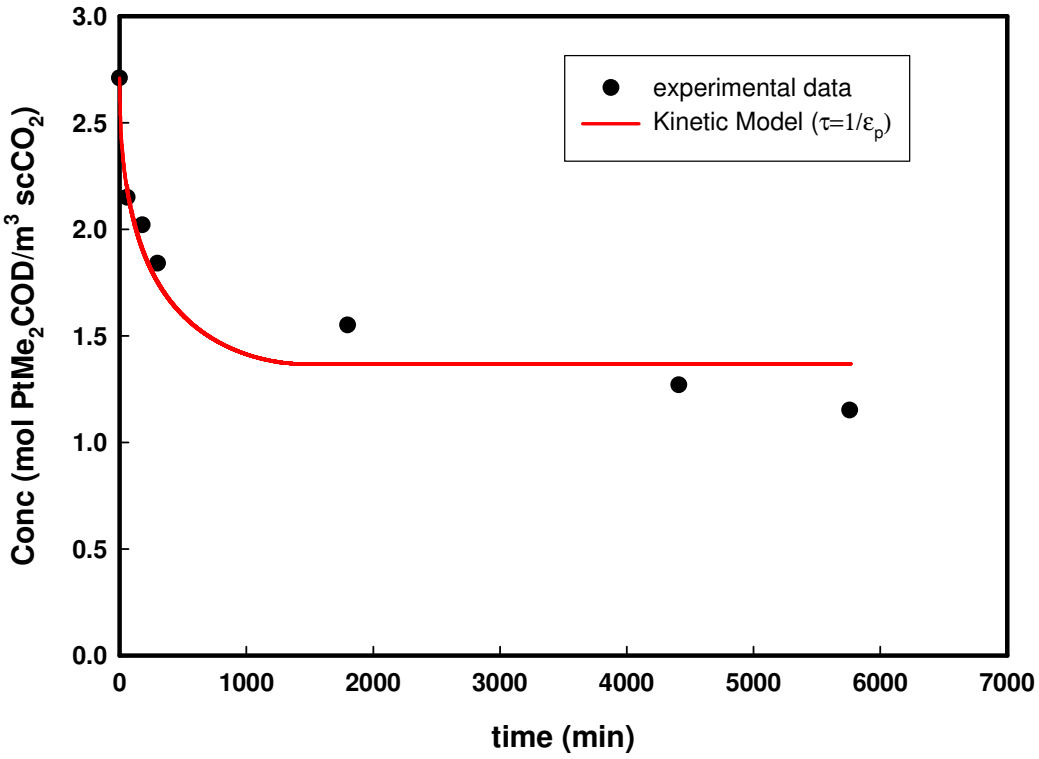

Figure 4.6: Experimental data and adsorption kinetics model,
Initial concentration= 2.71 mol $PtMe_2COD/m^3$ $scCO_2$, m_{RFA8}= 51.5 mg

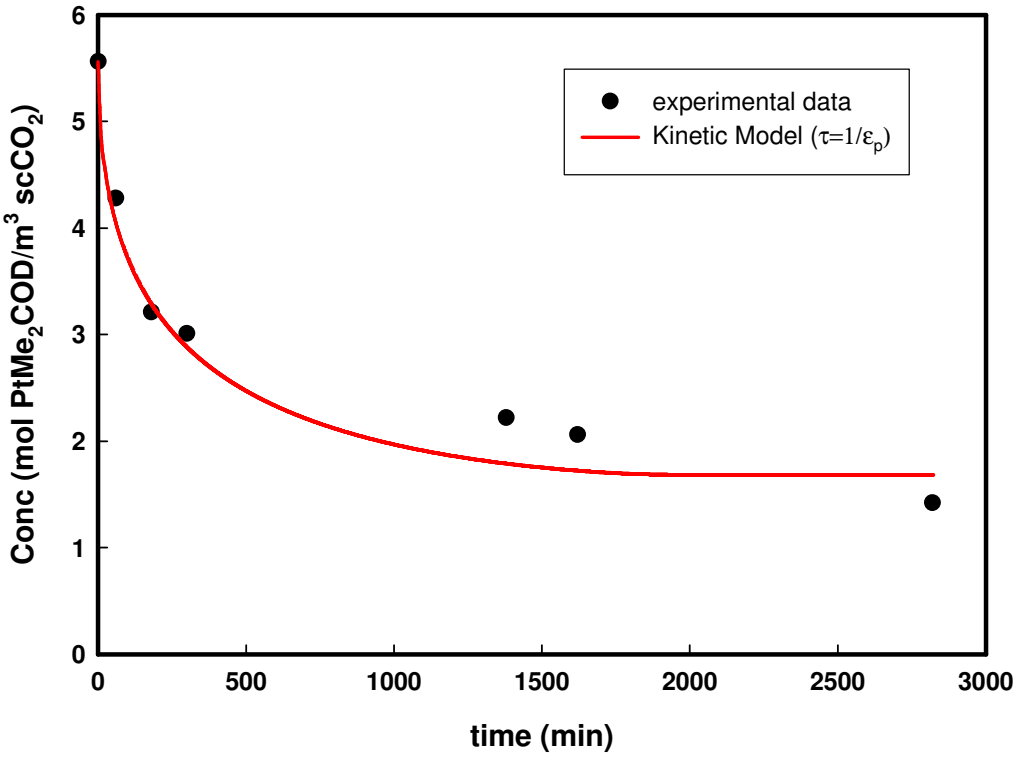

Figure 4.7: Experimental data and adsorption kinetics model,
Initial concentration= 5.56 mol $PtMe_2COD/m^3$ $scCO_2$, m_{RFA8}= 148.8 mg

The effect of the adjustable parameter "tortuosity" on the adsorption kinetics was also investigated using the model. Figure 4.8 shows that, as the tortuosity value decreases it takes shorter time to reach equilibrium. However, for each tortuosity value, the equilibrium concentrations are the same.

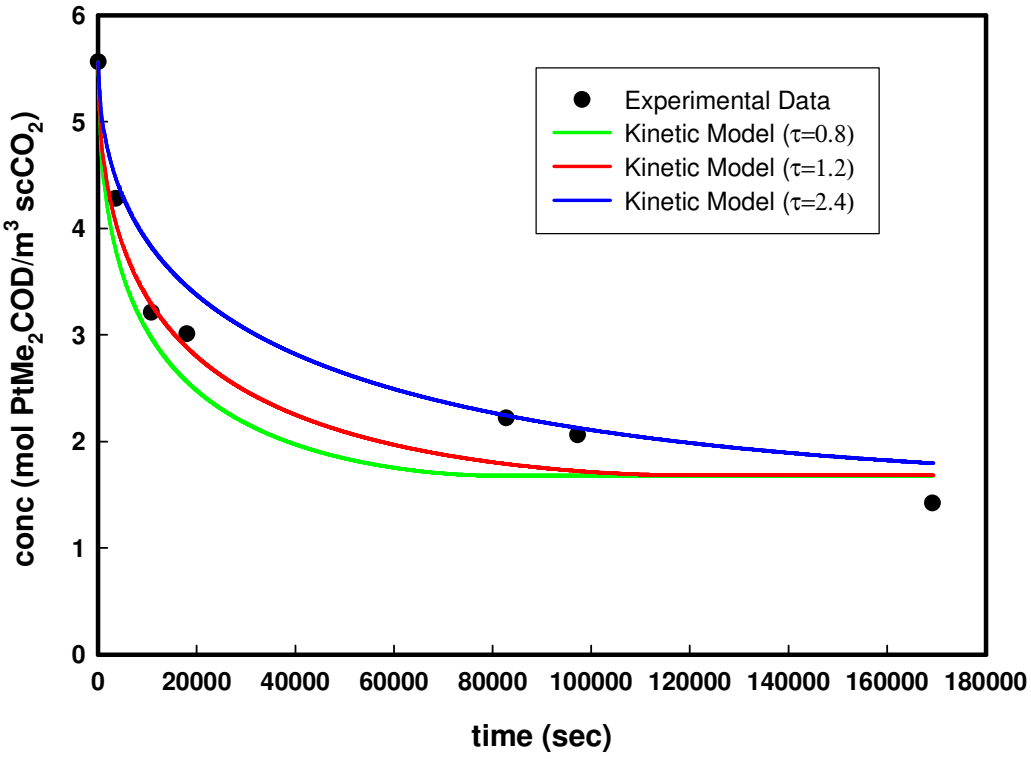

Figure 4.8: Effect of tortuosity on adsorption kinetics

The particle size of the adsorbent is an important parameter considering the adsorption kinetics. The effect of particle size of the spherical RFA8 to the adsorption kinetics is presented in Figure 4.9 which shows the model results that are obtained by using two different radii. As it can be seen from the figure, the time to reach equilibrium increases by increasing radius. It is also seen from the figure that the equilibrium concentrations are not the same. The reason for this is the different masses of the two particles. RFA8 particle with a smaller radius has a smaller mass and as it is mentioned before, with decreasing mass, the uptake amount decreases and thus the equilibrium concentration increases.

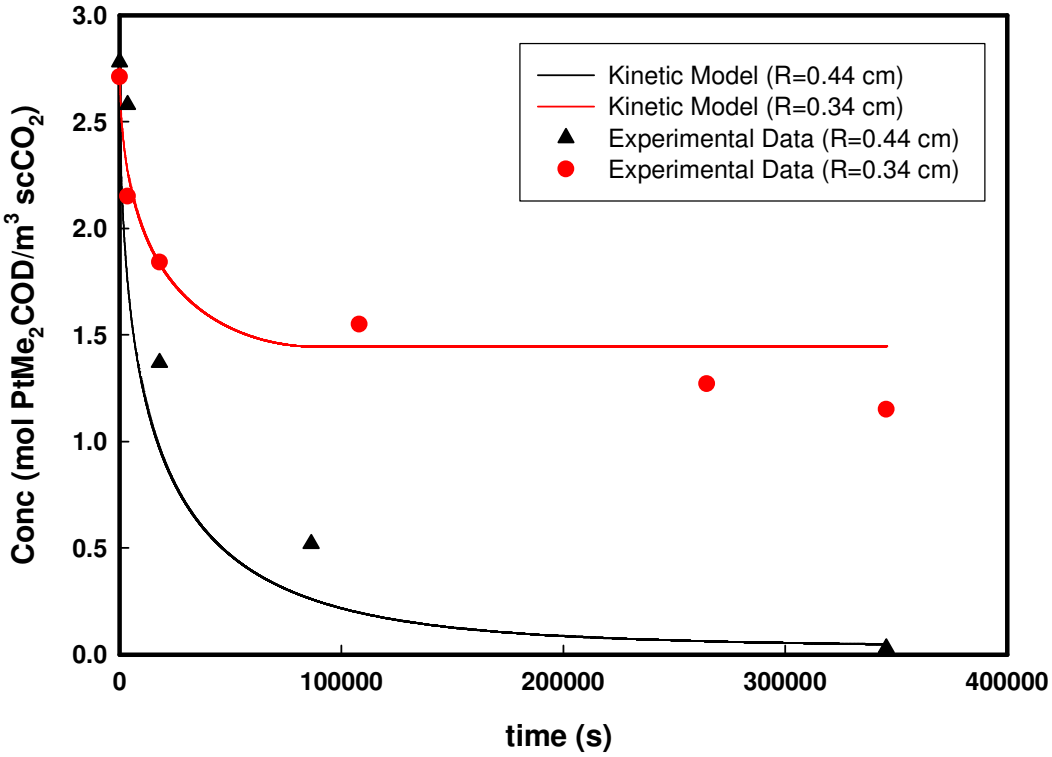

Figure 4.9: The effect of particle size on adsorption kinetics

4.4. Pt/RFA8 Particles

Pt/RFA8 particles were synthesized by reducing the adsorbed $PtMe_2COD$ molecule to its metal form. The reduction experiments have been conducted at 200°C under flowing H_2 for four hours. After reduction was completed, N_2 was passed through the reduced particles at 250°C in order to break the chemical bonds that were formed between Pt and H_2 during reduction. Pt/ RFA8 particles with three different Pt loadings 10 wt. %, 22 wt % and 34 wt. % were synthesized. The effect of metal loading on particle size of the synthesized particles was investigated by analyzing them in XRD. Figure 4.10 gives the XRD results of the three different metal loaded synthesized

particles. The average particle size of the synthesized particles was calculated by using Scherrer formula.

$$d_{XRD} = \frac{0.9\lambda_w}{\beta_{1/2}\cos\theta} \tag{4.15}$$

where d_{XRD} is the average particle size (nm), λ_w is the wavelength of the X-ray (0.15406 nm). $\beta_{1/2}$ is the width (radians) of the peak at half height and θ is the angle at peak maximum. $\beta_{1/2}$ and θ were determined by using the (111) peaks for each of the synthesized particles. As it can be seen from the figure, the broadest peak is seen at the lowest metal load which indicates the smallest particle size. The relation between particle size and the metal load of the synthesized particles is given in Figure 4.11. It is seen from the figure that, the particle size increases linearly with increasing metal load.

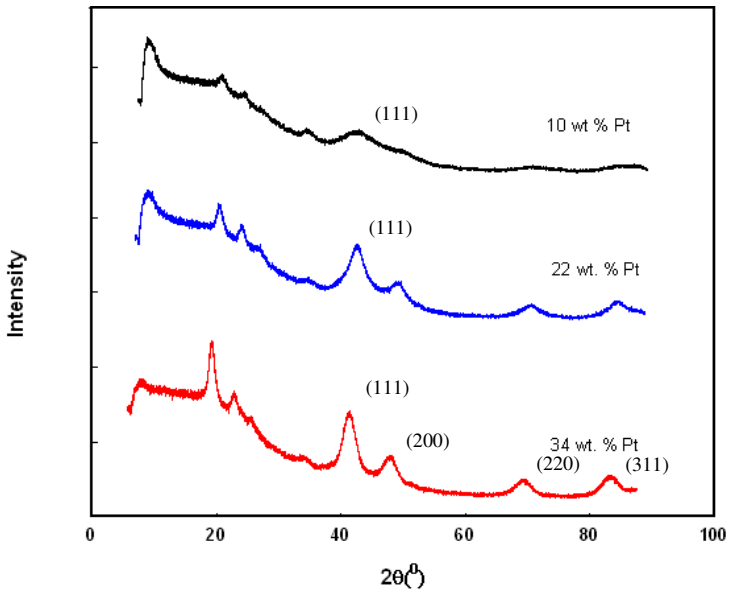

Figure 4.10: XRD spectra of different metal loaded Pt/RFA8 particles

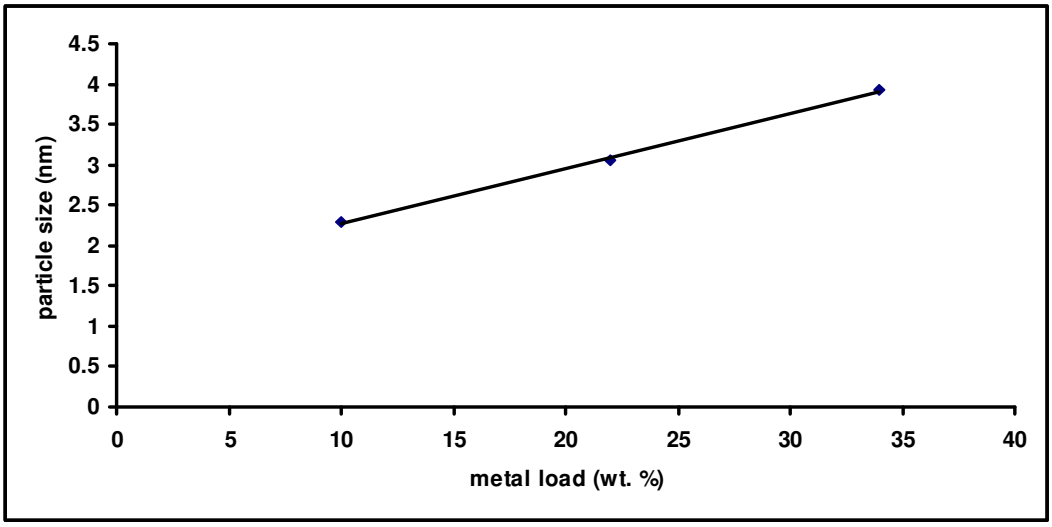

Figure 4.11: The effect of metal load on the particle size of Pt particles

Chapter 5

CONCLUSIONS AND FUTURE WORK

Supercritical CO_2 deposition technique is a promising and alternative technique to prepare supported metal nanoparticles. The preparation of supported nanoparticles with $scCO_2$ deposition technique include four successive steps which are the dissolutining of a metallic precursor in $scCO_2$, the exposure of the $scCO_2$-metallic precursor solution to the porous support, the adsorption of the metallic precursor on the surface of the support from $scCO_2$ and finally reduction of the metallic precursor to its metal form. The adsorption step is important since it affects the important properties of nanoparticles such as metal loading on the support, size of the particles and distribution of the particles on the support. The thermodynamics and kinetics of adsorption are the two important phenomenons that should be investigated.

In this thesis, the thermodynamics and kinetics of adsorption of $PtMe_2COD$ on RFA8 was investigated by developing a new experimental method. The method enabled us to analyze the supercritical phase. The thermodynamics of adsorption was described through adsorption isotherm of $PtMe_2COD$- $scCO_2$- RFA8 system. The adsorption isotherm was measured at 20.7 MPa and 60°C and represented by Langmuir model. The kinetics of adsorption of PtMe2COD on spherical RFA8 at 20.7 MPa and 60°C was investigated. A mass transfer model was developed in order to describe the adsorption kinetics and a good agreement of the model with the experimental data was observed. The effect of particle size of the RFA8 was investigated and it was seen that the time to reach equilibrium was shorter with a smaller particle size. The effect of adjustable parameter tortuosity to the kinetics of adsorption was also investigated. The time to reach equilibrium decreased with decreasing tortuosity.

In this thesis, Pt nanoparticles supported on resorcinol-formaldehyde aerogel (RFA8) was also prepared using $scCO_2$ deposition technique. Platinum dimethyl cyclooctadiene ($PtMe_2COD$) was used as the metallic precursor. The precursor was reduced thermally at 200°C for the different metal loaded particles. XRD measurements were done for the average particle sizes of the nanoparticles. XRD results showed that, the particle size of the nanoparticles increased with increasing metal load.

As a future work of this research, the adsorption isotherms can be measured at different pressures and temperatures, thus the effect of temperature and pressure on the behavior of the adsorption isotherm can be investigated. Furthermore, adsorption isotherms for binary systems can be measured using the same experimental technique. For the kinetic study, the mass transfer model can also be improved for binary systems. For further characterization of the supported nanoparticles, the effect of reduction temperature on the particle size and distribution can be investigated. The concentration gradient of the particles from the surface through the center of the support can also be investigated.

APPENDIX A

MATLAB Programme

```
function dCA=langmuir (t,CA)
global n;
m =   1038e-7;
R =   435e-5;
Vrfa=(4/3)*pi*R^3;
Gp =    m/Vrfa;
S =   3/Gp/R;
ds =  6e-10;
dp =  8e-9;
lamda = ds/dp
Flamda= 103e-2* exp((-4.5*lamda))
Vtot = 245e-5*m;
Ep =   Vtot/Vrfa
Dab =  132e-10;
to =  1/Ep;
Dep =  Flamda*Ep*Dab/to
V = 54e-6;
deltar = R/n;
k1 = 309.9564;
Q0 = 1.4082;
dCA= zeros (n,1);
dCA(1)= m*S*Dep/(-V)*(CA(1)-CA(2))/deltar;
for i=2:n-1
dCA(i)=  Dep/ (Ep+ Gp* k1*Q0/(1+k1*CA(i))^2) * ( (CA(i+1)-
2*CA(i)+CA(i-1))/(deltar^2)+2/(R-(i-1)*deltar)*(CA(i-1)-
CA(i+1))/2/deltar);
end
for i=n
dCA (i)= Dep/ (Ep+ Gp* k1*Q0/(1+k1*CA(i))^2) * ( (CA(i)-2*CA(i)+CA(i-
1))/(deltar^2)+2/(R-(i-1)*deltar)*(CA(i-1)-CA(i))/2/deltar);
end

% main program

clear all;
close all;
clc;
global n;
n=100;
init=zeros(n,1);
init(1,1)=5.56;
a=init';
options = odeset('RelTol',1e-5,'AbsTol',1e-5);
[T,Y] = ode15s(@langmuirexp24,[0:600:300000],a,options);
plot(T,Y(:,:)
```

APPENDIX B

Material Balance on a spherical adsorbent particle:

Volume of the adsorbent $= V = 4\pi r^2 \Delta r$

Fluid phase volume of the adsorbent $= V_F = 4\pi r^2 \Delta r \varepsilon_p$

In − Out + Generation = Accumulation

$$N_A\Big|_r \cdot 4\pi r^2 - N_A\Big|_{r+\Delta r} 4\pi (r+\Delta r)^2 = \frac{\partial (C_A V_F)}{\partial t} + \rho_p \frac{\partial q}{\partial t} V$$

$$N_A\Big|_r \cdot 4\pi r^2 - N_A\Big|_{r+\Delta r} 4\pi (r+\Delta r)^2 = \varepsilon_p \cdot 4\pi r^2 \Delta r \frac{\partial C_A}{\partial t} + \rho_p 4\pi r^2 \Delta r \frac{\partial q}{\partial t}$$

Dividing the equation by $4\pi \Delta r$

$$-\left(\frac{N_A\Big|_{r+\Delta r} r^2 - N_A\Big|_r r^2}{\Delta r} \right) = \varepsilon_p \cdot r^2 \frac{\partial C_A}{\partial t} + \rho_p r^2 \frac{\partial q}{\partial t}$$

$$-\frac{\partial}{\partial r}\left(N_A r^2\right) = \varepsilon_p r^2 \frac{\partial C_A}{\partial t} + \rho_p r^2 \frac{\partial q}{\partial t}$$

$$-\frac{\partial}{\partial r}\left(-De_{,p} \frac{dC_A}{dr} \cdot r^2\right) = r^2\left(\varepsilon_p \frac{\partial C_A}{\partial t} + \rho_p \frac{\partial q}{\partial t}\right)$$

$$De_{,p} \frac{\partial^2 C_A}{\partial r^2} \cdot r^2 + 2r \cdot De_{,p} \frac{\partial C_A}{\partial r} = r^2\left(\varepsilon_p \frac{\partial C_A}{\partial t} + \rho_p \frac{\partial q}{\partial t}\right)$$

$$r^2 De_{,p}\left(\frac{\partial^2 C_A}{\partial r^2} + \frac{2}{r} \frac{\partial C_A}{\partial r}\right) = r^2\left(\varepsilon_p \frac{\partial C_A}{\partial t} + \rho_p \frac{\partial q}{\partial t}\right)$$

$$\varepsilon_p \frac{\partial C_A}{\partial t} + \rho_p \frac{\partial q}{\partial t} = De_{,p}\left(\frac{\partial^2 C_A}{\partial r^2} + \frac{2}{r} \frac{\partial C_A}{\partial r}\right)$$

BIBLIOGRAPHY

[1] Burda, C.; Chen, X.; Narayanan, R.; EI-Sayed, M. A. Chemistry and properties of nanocrystals of different shapes. *Chem. Rev* **2005** , *105*, 1025

[2] A.L. Dantas, P.D. Alves, D.Arando, M. Schmal, Characterization of Carbon Supported Pd Catalysts: Influence of Electronic and Particle Size Effects Using Reaction Probes, Appl. Catal. 277 (2004) 71-81.

[3]M.Markus, M.Kumar, K.Eklund, H.Sjöholm, S.Munzin, Hydrogenolysis of Hydroxymatairesol over Carbon Supported Palladium Catalysts, Catal. Letters 1103 (2005) 125-131.

[4] H.Li, G.Sun, N.Li, S.Sun, D.Su, Q.Xin, Design and Preparation of Highly Active Pt-Pd/C Catalyst for the Oxygen Reduction Reaction, J.Phys.Chem. 111 (2007) 5605-5617.

[5] H. Jinnai , T. Kaneko , H.Nishioka , H. Hasegawa , T. Nishi, Spatial Arrangement of Metal Nanoparticles Supported by Porous Polymer Substrates Studied by Transmission Electron Microtomograph, Chemical Record, 6, (2006), 267-274

[6] B Basu, S Das, P Das, B Mandal, D Banerjee , F Almqvist, Palladium Supported on a Polyionic Resin as an Efficient, Ligand-Free, and Recyclable Catalyst for Heck, Suzuki-Miyaura, and Sonogashira Reactions, Synthesis-Stutgart, 7, (2009), (1137-1146)

[7] A. Drelinkiewicz , J. W. Sobczak , E Sobczak , M Krawczyk , A Zieba , A. Waksmundzka-Gora , Physicochemical and Catalytic Properties of Pt-poly(4-vinylpyridine) Composites, Materials Chemistry and Physics, 114, (2009), 763-773

[8] Y.Gao, C. A. Chen,H. M. Gau, J. A. Bailey, E. Akhadov, D. Williams and H. L. Wang, Facile Synthesis of Polyaniline-Supported Pd Nanoparticles and Their Catalytic Properties toward Selective Hydrogenation of Alkynes and Cinnamaldehyde, Chem. Mater., 20, (2008), 2839–2844.

[9] P. Claus, A. Bru1ckner, C. Mohr and H. Hofmeister, Supported Gold Nanoparticles from Quantum Dot to Mesoscopic Size Scale: Effect of Electronic and Structural

Properties on Catalytic Hydrogenation of Conjugated Functional Groups, J. Am. Chem. Soc. 122, (2000), 11430-11439.

[10] Y. Mizukoshi, S. Seino, K. Okitsu, T. Kinoshita, Y. Otome, T. Nakagawa, T. A. Yamamoto, Sonochemical preparation of composite nanoparticles of Au/c-Fe_2O_3 and magnetic separation of glutathione, Ultrasonics Sonochemistry, 12, (2005), 191–195.

[11] J.M. Miller, B. Dunn, T.D. Tran, R.W. Pekala, Deposition of ruthenium nanoparticles on carbon aerogels for high energy density supercapacitor electrodes, J. Electrochem. Soc. 144 (1997) L309.

[12] S. Papp, A. Szücs and I. Dékány, Preparation of Pd^0 nanoparticles stabilized by polymers and layered silicate, Applied Clay Science, 19, (2001), 155–172.

[13] C. Erkey, Preparation of Metallic Supported Nanoparticles and Films Using Supercritical Fluid Deposition. J. Supercrit. Fluids , 47, (2009), 517-522

[14] J.J. Watkins., T.J. McCarthy, Polymer/metal Nanocomposite Synthesis in Supercritical CO_2. Chem. Mater. 7, (1995), 1991-1994.

[15] R. Jiang, Y. Zhang, S. Swier, X.Wei, C. Erkey, H.R. Kunz, J.M. Fenton, Preparation via supercritical fluid route of Pd-impregnated Nafion® membranes that exhibit reduced methanol crossover for direct methanol fuel cells, Electrochem. Solid State Lett., 8, (2005), A611.

[16] E. Said-Galiyev, L. Nikitin, R. Vinokur, M. Gallyamov, M. Kurykin, O. Petrova, B.Lokshin, I. Volkov, A. Khokhlov, K. Schaumburg, Newchelate complexes of copper and iron: synthesis and impregnation into a polymer matrix from solution in supercritical carbon dioxide, Ind. Eng. Chem. Res. 39 (2000) 4891.

[17] S.K. Morley, P.C. Marr, P.B.Webb, A.R. Berry, F.J. Allison, G. Moldovan, P.D. Brown, S.M. Howdle, Clean preparation of nanoparticulate metals in porous supports: a supercritical route, J. Mater. Chem., 12, (2002), 1898-1905.

[18] T. Hasell, L. Lagonigro, A.C. Peacock, S. Yoda, P.D. Brown, P.J.A. Sazio, S.M. Howdle, Silver nanoparticle impregnated polycarbonate substrates for surface enhanced Raman spectroscopy, Adv. Funct. Mater., 18, (2008), 1265.

[19] B. Wong, S. Yoda, S.M. Howdle, The preparation of gold nanoparticle composites using supercritical carbon dioxide, J. Supercrit. Fluids, 42, (2007), 282-287.

[20] Y. Zhang, C. Erkey, Preparation of Supported Metallic Nanoparticles Using Supercritical Fluids: A Review. J.Supercrit. Fluids, 38, (2006), 252-267.

[21] Y. Zhang, B. Cangul,; Y. Garrabos, C. Erkey, Thermodynamics and Kinetics of Adsorption of Bis(2,2,6,6-tetramethyl-3,5-heptanedionato) (1,5-cyclooctadiene) Ruthenium(II) on Carbon Aerogel from Supercritical CO_2 Solution, J. Supercrit. Fluids 44, (2008), 71-77.

[22] C. D. Saquing, D. Kang,; M. Aindow,; C. Erkey, Investigation of the Supercritical Deposition of Platinum Nanoparticles into Carbon Aerogels. Micropor. Mesopor. Mater. 80, (2005), 11-23.

[23] O. Aschenbrenner, N. Dahmen, K. Schaber, E. Dinjus, Adsorption of Dimethyl(1,5- cyclooctadiene) Platinum on Porous Supports in Supercritical Carbon Dioxide. *Ind. Eng*. Chem. Res., 47, (2008), 3150-3155.

[24] F. Cansell , C. Aymonier, A. Loppinet-Serani, Review on materials science and supercritical fluids, Current Opinion in Solid State and Materials Science, 7, (2003), 331–340.

[25] F. Cansell, B. Chevalier, A. Demourgues, J. Etourneau, C. Even, Y. Garrabos, V. Pessey, S. Petit, A. Tressaud and F Weill, Supercritical fluid processing: a new route for materials synthesis, J. Mater. Chem., 9, (1999), 67–75

[26] G. Brunner, M. Johannsen, New aspects on adsorption from supercritical fluid phases, J. of Supercritical Fluids, 38, (2006), 181–200

[27] D.D. Do, Adsorption Analysis, Equilibria and Kinetics, Vol.2 , Imperial College Press, London, (1998),

[28] S. Diankov, D. Barth, A. Vega-Gonzalez, I. Pentchev, P. Subra-Paternault, Impregnation isotherms of hydroxybenzoic acid on PMMA in supercritical carbon dioxide, J. of Supercritical Fluids, 41, (2007), 164–172

[29] C. Erkey, G. Madras, M. Orejuela, A. Akgerman, Supercritical Carbon Dioxide Extraction of Organics from Soil, Environ. Sci. Technol., 27, (1993), 1225-1231.

[30] G. Madras, C. Erkey, A. Akgerman, Supercritical extraction of organic contaminants from soil combined with adsorption onto activated carbon, Environ. Prog., 13, (1994), 45-50.

[31] M. Cross Jr., A. Akgerman, Adsorptive separations using supercritical frontal analysis chromatography, AIChE J., 44, (1998), 1542–1554.

[32] P. Subra, A. Vega-Bancel, E. Reverchon, Breakthrough curves and adsorption isotherms of terpene mixtures in supercritical carbon dioxide, Journal of Supercritical Fluids, 12, (1998), 43-57.

[33] R. Harikrishnan, M.P. Srinivasan, C.B. Ching, Adsorption of ethyl benzene on activated carbon from supercritical CO_2, AIChE J., 44, (1998), 2620–2627.

[34] S. Lucas, M. J. Cocero, C. Zetzl and G. Brunner**,** Adsorption isotherms for ethylacetate and furfural on activated carbon from supercritical carbon dioxide, Fluid Phase Equilibria, 219, (2004), 171-179.

[35] H. Xing, B. Su, Q. Ren, Y. Yang, Adsorption equilibria of artemisinin from supercritical carbon dioxide on silica gel, J. of Supercritical Fluids, 49, (2009), 189-195.

[36] M. Lübbert, G. Brunner, M. Johannsen, Adsorption equilibria of α- and δ-tocopherol from supercritical mixtures of carbon dioxide and 2-propanol onto silica by means of perturbation chromatography, J. of Supercritical Fluids, 42, (2007), 180–188.

[37] Y. Han, Y. Yang and P. Wu, Adsorption Equilibria of cis-5,8,11,14,17 Eicosapentaenoic Acid Ethyl Ester and cis-4,7,10,13,16,19-Docosahexaenoic Acid Ethyl Ester from Supercritical Carbon Dioxide on Silica Gel, J. Chem. Eng. Data, 53, (2008), 16–19

[38] S. Peper, M. Lübbert, M. Johannsen, G. Brunner, Separation of ibuprofen enantiomers by supercriticial fluid simulated moving bed chromatography, Sep. Sci. Technol., 37, (2002), 2545–2566.

[39] I. Smirnova, J. Mamic and W. Arlt, Adsorption of Drugs on Silica Aerogels, Langmuir, 19, (2003) , 8521-8525

[40] W.H. Cheung, Y.S. Szeto, G. McKay, Intraparticle diffusion processes during acid dye adsorption onto chitosan, Bioresource Tech., 98, (2007), 2897–2904.

[41] Q. Sun, L. Yang, The adsorption of basic dyes from aqueous solution on modified peat–resin particle, Water Res., 37, (2003), 1535-1544.

[42] C. Long, A. Li, H. Wu, Q. Zhang, Adsorption of Naphthalene Onto Macroporous and Hypercrosslinked Polymeric Adsorbent: Effect of Pore Structure of Adsorbents on Thermodynamic and Kinetic Properties, Colloids and Surfaces A: Physicochem. Eng. Aspects, 333, (2009), 150–155.

[43] R.W. Pekala, Organic Aerogels from the Polycondensation of Resorcinol with Formaldehyde, Journal of Materials Science, 24, (1989), 3221-3227.

[44] J.M. Smith, Chemical Engineering Kinetics, 2nd ed., McGraw-Hill, Tokyo, (1970), 317- 465

[45] Fogler, H.Scott , Elements of Chemical Reaction Engineering, 3rd Ed., Prentice-Hall International Inc., New Jersey , (1999), 739-741.

[46] T. Funazukuri, C.Y. Kong, S.Kagei, Impulse response techniques to measure binary diffusion coefficients under supercritical conditions, J. Chromotogr. A, 1037, (2004), 411-429